Titre: Title:	High-Temperature Oxidation Protection of γ-Based TiAl by Sputtered AlOF Films
Auteur: Author:	Florence Bergeron
Date:	2019
Type:	Mémoire ou thèse / Dissertation or Thesis
Référence: Citation:	Bergeron, F. (2019). High-Temperature Oxidation Protection of γ-Based TiAl by Sputtered AlOF Films [Mémoire de maîtrise, Polytechnique Montréal]. PolyPublie. https://publications.polymtl.ca/3849/

UNIVERSITÉ DE MONTRÉAL

HIGH-TEMPERATURE OXIDATION PROTECTION OF γ-BASED TIAL BY SPUTTERED ALOF FILMS

FLORENCE BERGERON
DÉPARTEMENT DE GÉNIE PHYSIQUE
ÉCOLE POLYTECHNIQUE DE MONTRÉAL

MÉMOIRE PRÉSENTÉ EN VUE DE L'OBTENTION
DU DIPLÔME DE MAÎTRISE ÈS SCIENCES APPLIQUÉES
(GÉNIE PHYSIQUE)
AVRIL 2019

UNIVERSITÉ DE MONTRÉAL

ÉCOLE POLYTECHNIQUE DE MONTRÉAL

Ce mémoire intitulé :

HIGH-TEMPERATURE OXIDATION PROTECTION OF γ-BASED TIAL BY SPUTTERED ALOF FILMS

présenté par : BERGERON Florence
en vue de l'obtention du diplôme de : Maîtrise ès sciences appliquées
a été dûment accepté par le jury d'examen constitué de :

M. WERTHEIMER Michael, Ph. D., président
Mme SAPIEHA Jolanta-Ewa, Ph. D., membre et directrice de recherche
M. MARTINU Ludvik, Ph. D., membre et codirecteur de recherche
M. TAVARES Jason Robert, Ph. D., membre

DEDICATION

To my parents,
for your constant and invaluable suport

ACKNOWLEDGEMENTS

I would first like to thank my advisors Jolanta-Ewa Klemberg- Sapieha and Ludvik Martinu. Their great experience as thin film scientists and as supervisors has been invaluable to me.

Secondly, many thanks to Marjorie Cavarroc and Stephane Knittel, from Safran group, for sharing their expertise on industrial aerospace engineering. I also express my gratitude to Michael Wertheimer, jury president, and to Jason Robert Tavares, jury member, for taking the time to review and evaluate my work.

For taking me under his wing, sharing his impressive knowledge of plasma processes, and for being a supportive mentor, I thank Simon Loquai. You have been a key to the success of my Master's project.

I would also like to thank my colleagues who were working with me on this project, more specifically Etienne Bousser for his thoughtful supervision and support, and Josefina Crespo-Villegas, for the companionship and in and out of the laboratory. This project would not have gone very far without the help of exceptional technicians. I thank Francis Turcot, Francis Boutet, Samuel Cardinal, and Sébastien Chénard for their expert help in the laboratory.

It goes without saying that I thank all my colleagues at the FCSEL. A sincere thank you to Oleg Zabeida for his help with plasma diagnostics, to Thomas Schmitt for his help on XRD, and also to Francis Blanchard, Erika Herrera, Jacques Lengaigne, Yuxiao Wu, Rodrigue Beaini, Antonin Riera, Bill Baloukas, Veronika Simova, Amaury Kilicaslan, Michael Laberge, Jincheng Qian, Stephen Brown, Sasha Woodward, Sourouch Hafezian, Erwens Broustet, Fabrice Pougoum, Louis Dubé Riopelle, Philip Rumsby, Anna Jedrzejczak, Julien Gagnon, Frédérik Poitevin, Julien Schmitt.

Many thanks to Josianne Lefebvre for the expert XPS measurements, to Martin Chicoine and his skilled RBS measurements, and to Philippe Plamondon for his training and kind support on the SEM.

I would finally like to thank my family for their support, and Raphaël, who was always there for me.

RÉSUMÉ

Les aluminures de titane (TiAl) ont récemment été introduits dans la confection de lames de turbine basse-pression chez certains fournisseurs de réacteurs d'avion. Leur force et leur module d'Young spécifiques se comparent à ceux des alliages de nickel présentement utilisés en industrie, mais leur faible densité permet de réduire le poids des lames et des pièces les soutenant. Une telle réduction du poids des moteurs mène à des économies de carburant intéressantes, qui se traduisent ultimement par la réduction des coûts d'opération et des émissions polluantes. Il est cependant difficile d'utiliser le TiAl dans des étages des moteurs autres que les turbines basse-pression, où les températures sont somme toute basses, puisque qu'il s'oxyde rapidement lorsqu'exposé à des températures supérieures à 750 °C. L'objectif du projet présenté dans ce mémoire est de prévenir l'oxydation à haute température du TiAl en utilisant des revêtements pulvérisés fluorés.

La présence de fluor dans les revêtements permet l'utilisation de l'effet halogène, un moyen efficace de protéger le TiAl contre l'oxydation. En effet, lorsqu'exposé aux hautes températures d'opération, il y a formation de fluorures d'aluminium sous l'interface du TiAl, suivie de leur diffusion jusqu'à la surface et de leur oxydation, ce qui crée une couche protectrice d'oxyde d'aluminium. Cet oxyde est reconnu pour son imperméabilité à l'oxygène, ce qui permet de protéger le TiAl de l'oxydation future.

Les travaux présentés dans ce mémoire portent sur la production de revêtements fluorées d'oxy-fluorure d'aluminium par pulvérisation magnétron réactive dans une atmosphère de CF_4 et de O_2. La chimie du plasma réactif est monitorée par spectrométrie de masse. La puissance de pulvérisation et l'apport en oxygène dans le plasma réactif sont variés pour comprendre leurs effets sur la composition chimique du plasma. La composition des revêtements d'AlOF est ensuite à son tour mesurée, à l'aide de la spectroscopie de rétrodiffusion de Rutherford. Les relations entre cette composition et celle du plasma réactif sont ainsi établies. Finalement, différents revêtements d'AlOF à la composition connue sont oxydés pour déterminer leur capacité à protéger le TiAl. Pendant ces tests d'oxydation, les échantillons sont pesés pour monitorer leur prise de masse. Des tests d'oxydation sont effectués à différentes températures, pour caractériser leur cinétique d'oxydation.

Ces travaux démontrent que les revêtements d'AlOF protègent efficacement le TiAl contre l'oxydation à haute température. Les prises de masses sont faibles (sous 0.5 mg cm^{-2} après 50 h d'oxydation à 875 °C) et les taux d'oxydations sont amoindris par la présence d'AlOF. L'oxyde résultant est principalement composé d'oxyde d'aluminium, contrairement

aux échantillons non-traités qui ont une prise de masse importante et une couche d'oxyde composée à la fois de TiO_2 et de Al_2O_3.

ABSTRACT

Titanium aluminides are intermetallic compounds of great interest to the automotive and aerospace industries. Indeed, being low-density alloys with high strength, their specific mechanical properties like specific strength or specific elastic modulus make them suitable for applications that were until now dominated by Ni-bases alloys. The introduction of TiAl in turbine and compressor blades instead of other heavy alloys contribute to the weight reduction effort made by engine designers, to optimize the thrust-to-weight ratio of their aircraft. Large-scale implementation of TiAl in airplane engines is however limited by its severe oxidation at temperatures higher then 750 °C. The goal of the present work is to protect TiAl against such oxidation through the combined use of sputtered thin films and the halogen effect.

The halogen effect requires that a halogen, in this case, fluorine, is applied to the surface of TiAl to promote the formation of gaseous aluminum fluorides. These fluorides migrate to the surface of the TiAl during high-temperature oxidation, where they are oxidized into aluminum oxide, a dense, protective and durable oxidation barrier. The detrimental oxidation of the TiAl is then blocked.

This works reports on the deposition of aluminum oxy-fluoride coatings by reactive magnetron sputtering. The sputtering process is monitored by mass spectrometry, to gain insight into the gas phase chemistry of the reactive plasma. The chemical composition of the sputtered coatings is then measured by Rutherford backscattering spectrometry, and a relationship between the composition of the coatings and the composition of the plasma is established. Finally, AlOF coatings of different compositions are oxidized, to determine which coating composition offers the best oxidation protection. Mass gains are measured throughout the isothermal oxidation tests, which were performed at different temperatures to study the oxidation kinetics of the AlOF coatings. Samples' surface and cross sections were observed before and after oxidation by scanning electron microscopy and energy dispersive x-ray spectroscopy.

It was found that the coatings efficiently protect the TiAl against high-temperature oxidation. The mass gains of coated samples are significantly reduced in comparison to those of unprotected TiAl. The oxidation kinetics are slowed while the oxidation activation energy is increased. An alumina scale is growing on protected TiAl.

TABLE OF CONTENTS

LIST OF TABLES

LIST OF FIGURES

LIST OF SYMBOLS AND ACRONYMS

α	Sticking coefficient
BLI^2	Beamline ion implantation
CTE	coefficient of thermal expansion
DC	Direct current
ΔM	Mass gain per unit area or per unit time
EDS	Energy dispersive x-ray spectroscopy
FCSEL	Functional Coating and Surface Engineering Laboratory
GE	General electric
HiPIMS	High power impulse magnetron sputtering
IATA	International Air Transport Association
$J_{\text{Al}}^{\text{ox}}$	Aluminum flux into the Al oxide
k_B	Boltzmann constant
k_n	Oxidation rate constant
LPT	Low-pressure turbine
m	Mass
MS	Mass spectrometry/spectrometer
n	Oxidation exponent
N_A	Avogadro constant
OP-S	Oxide polishing suspension
P	Partial pressure
$P_{\text{AlF}}^{\text{min}}$	Minimal Al-halide partial pressure
PI^3	Plasma immersion ion implantation
PVD	Physical vapor deposition
Q	Activation energy
R	Ideal gas constant
RF	Radio frequency
RGA	Residual gas analysis
SEM	Scanning electron microscope
T	Temperature
t	Time
TGA	Thermogravimetric analysis
XRD	X-ray diffraction

CHAPTER 1 INTRODUCTION

The 21st century is one of major importance for the aerospace industry because of the important increase in flight demands from the Asian market, driven mostly by China, India, and Indonesia. Evaluated at 3.8 billion in 2016 by the International Air Transport Association (IATA), the number of airplane passengers is predicted to double by 2037, reaching 8.2 billion [5]. To supply to the rising demand, to mitigate operation costs, and to reduce the environmental impact of such air traffic, aircraft designs are pushed to technological limits. This is particularly true for the engines, whose efficiency is dictated by their thrust-to-weight ratio. Judicious weight reduction combined with the elevation of engines' operating temperatures will therefore improve their efficiency.

1.1 Titanium aluminides as innovative intermetallic alloys

In this context of growth and efficiency, titanium aluminides (TiAl) attract immense interest because of their low weight and their high specific strength at high temperature compared to conventional titanium or nickel alloys [6, 7]. This allows for the manufacture of lighter blades and allows the reduction of the mass of other components that would otherwise have to support the heavy blades [8].

Their implementation in industry began in the automotive sector, with the arrival of TiAl-containing turbochargers in the Mitsubishi's Lancer 6 in 1999 [7, 8], followed by production of TiAl valves for Formula One engines in 2002. The first use of TiAl in an aircraft engine occurred in 2011, in General Electric's (GE) GEnx engine. The last two stages of its low-pressure turbine (LPT) were made of Ti-48Al-2Nb-2Cr (48-2-2), a titanium aluminide alloyed with 2 at.% of niobium and chromium [6]. This alloy is one of the most widely used TiAl, with more than 725 tons of 48-2-2 produced up to 2016, dispatched on more than 300 Boeing aircraft powered by the GEnx engine [6]. In addition to GE, SNECMA also introduced 48-2-2 in its LEAP™ engines, spreading the technology to some Airbus and Comac aircraft [6]. Pratt and Whitney and Rolls Royce have also announced that their own TiAl alloys would come on the market [6].

The overall performances of the GEnx engine speak for the effectiveness of TiAl. Reduction in fuel consumption of 20%, along with an 80% reduction in polluting NOx emissions, and a 50% noise reduction were attributed to the new engine, some of this being credited to TiAl [6]. The implementation of TiAl in engines by the four major engine manufacturers in

the world demonstrates the enthusiasm surrounding the alloy.

1.2 Problems surrounding oxidation of TiAl alloys

Like all technological alloys, titanium aluminides have some disadvantages that complicate their implementation. TiAls are difficult to fabricate, exhibit very low ductility at room temperature, and are susceptible to oxidation at high temperatures [7]. While the fabrication of quality TiAl with good ductility is primordial, this work will focus on the oxidation of TiAl at high temperatures. Indeed, in the context of increased operating temperatures for improved efficiency, it is a priority to ensure the good oxidation resistance of the TiAl. In its current form, TiAl (and specifically, TiAl 48-2-2) offers a good oxidation resistance when exposed to temperatures below 750 °C. This resistance is even better than conventional titanium alloys used in the industry which exhibit poor oxidation resistance due to their high Ti content [6, 9]. Temperature ranges for current TiAl application maintain the alloy in a safe range for oxidation.

TiAl becomes susceptible to oxidation damage above 750 °C, where the rapid oxidation of titanium compared to aluminum produces a brittle oxide scale composed of TiO_2 and Al_2O_3 [10]. Growing inward and as such, consuming the TiAl, this oxide scale is highly permeable to oxygen due to its high level of porosity and its susceptibility to cracking and spalling [10]. The oxidation is therefore persistent. In addition to oxidation, the unrelenting presence of oxygen at the surface of TiAl leads to oxygen dissolution in the TiAl, causing embrittlement of the alloy [11]. The TiAl oxidation will be covered in more details in section 2.2.3. For now, it suffices to say that it is a major obstacle for the application of TiAl to the next generation of high-temperature engines, and to their spread in other, hotter stages of the engines.

The initial solution to overcome TiAl oxidation was the addition of alloying elements in the TiAl. The most notable element is niobium, added in quantities ranging from 2 to 8 at.% [7, 9]. The drawback of this approach is that the composition of TiAl can only be modified within a very small margin. Indeed, the mechanical properties of the alloys are impacted by any modification of the composition [7]. A careful balance needs to be established, and this optimal balance is already attained for the latest generation of TiAl, with oxidation resistance reaching 750 °C [10].

To improve the resistance past 750 °C, another solution is required. Surface engineering, by decoupling bulk and surface properties, allows the protection of any alloy without impacting its carefully designed composition. This surface engineering is usually separated into three categories of processes: i) overlay coatings, ii) diffusion coatings, and iii) the halogen effect.

Their common goal is the formation of a protective oxygen barrier, often in the form of a dense oxide like α alumina [10].

In a recent review of surface engineering solutions, Pflumm and coworkers reported that the halogen effect allowed protection at the highest temperature and on a wide range of TiAl [10]. The halogen effect is based on the formation of aluminum halides at the surface of the TiAl that are preferentially oxidized to aluminum oxide at high temperature. This preferential oxidation suppresses the oxidation of titanium and allows the formation of a protective pure alumina scale. The most common halogen used is fluorine [12]. Surprisingly, no record of surface halogenation by a plasma deposition processes was found in the literature for the protection of TiAl. Halogen plasmas, in particular, fluorine plasmas, are well documented for applications in microelectronics, optics, and tribology. Plasma processes allow for the deposition of almost any metal, ceramic or polymeric material in the form of a thin film, with precise control over the coatings' chemical composition, structure, and mechanical, electrical or optical properties. For these reasons, it was decided to investigate the possibility to protect TiAl 48-2-2 with the halogen effect using plasma aluminum oxy-fluoride thin films deposited by reactive magnetron sputtering in an $Ar/O_2/CF_4$ atmosphere.

The sputtered films are composed of aluminum oxi-fluoride (AlOF). The presence of aluminum in the film ensures that it is an alumina former, i.e. that it oxidizes to aluminum oxide at high temperatures. As previously mentioned, aluminum oxide is an effective oxygen barrier. The presence of fluorine ensures that the halogen effect will take place. Oxygen is used in combination with the CF_4 to first increase the amount of reactive fluorine liberated by the fluorocarbon in the plasma. It is also expected to bind with carbon to form volatile carbon mono- and dioxide that will evaporate from coatings, preventing carbon contamination [13]. To ensure an optimal adhesion to the TiAl substrate, a thin aluminum bond coat is sputtered prior to the AlOF deposition.

Reactive magnetron sputtering is chosen as a deposition technique because of its versatility. Any compound that can be molded into a target can be sputtered by magnetron sputtering, and it is especially easy to do so with metals. The addition of reactive gases like oxygen, fluorocarbons, or nitrogen allows the deposition of compounds like oxides, nitrides, carbides, and halides. The specifics of (reactive) magnetron sputtering will be covered in section 2.4.1.

Great expertise in magnetron sputtering was developed in École Polytechnique de Montreal within the Functional Coating and Surface Engineering Laboratory (FCESL). Together with our industrial partner Safran Group, one of the major aircraft engine manufacturer and a leader in the development of TiAl alloys, it will be possible to develop an innovative solution to the high-temperature oxidation problem of titanium aluminides.

1.3 Objectives of the project

The main objective of the proposed project is to develop coatings that allow the use of intermetallic Ti-Al48-Nb2-Cr2 (48-2-2) at elevated temperatures (750 °C to 800 °C) by providing high oxidation resistance. Specifically, the goal is to apply the halogen effect to form a protective Al_2O_3 oxidation barrier. To quantify the level of oxidation protection offered by the AlOF coatings, the mass gain of the coated TiAl after oxidation will be monitored. To be considered protective, the coating will have to maintain the mass gain below 1 mg/cm^2 during an oxidation test of 50 h at 875 °C. To reach this global objective, the following specific objectives have been devised:

1. Deposit AlOF coatings containing at least 60 at.% of fluorine on TiAl by reactive magnetron sputtering;
2. Establish the relationship between different sputtering parameters (power and reactive gas flows) and the chemical composition of the plasma;
3. Demonstrate the relationship between the chemical species present in the plasma and the resulting chemical composition of the AlOF coatings;
4. Attest which coating composition protects TiAl the best against oxidation;

1.4 Scientific publications

In addition to this thesis, the results obtained from this study are currently being added to a patent, in close collaboration with Safran Group:

High-temperature oxidation resistance barrier for performance enhancement of the γ-TiAl alloy and method for making the same., 2019

Finally, this research will be presented at the International Conference on Metallurgical Coatings and Thin Films of 2019:

F. Bergeron, S. Loquai, E. Bousser, M. Cavarroc, S, Knittel, L. Martinu, and J.E Klemberg-Sapieha, *High-temperature oxidation protection of γ-based TiAl by sputtered AlOF films*, 2019.

1.5 Thesis outline

In Chapter 2, following this introduction, a literature review will present the necessary knowledge and theory to navigate through the rest of the thesis. This review will start with a survey

of titanium aluminides' properties and metallurgical composition. Emphasis will then be put on the mechanisms behind the oxidation of TiAl. The second part of the review will focus on the existing solutions to protect TiAl against oxidation. Overlay and diffusion coatings will be discussed briefly, while the halogen effect will be covered in depth as it is the solution of choice for this work. The third section of the review will cover plasma processes and plasma chemistry notions, including magnetron sputtering, reactive magnetron sputtering, and CF_4 plasma chemistry.

The third chapter of the thesis will be dedicated to the experimental methodology including the sample preparation steps, the deposition processes, the plasma diagnostic tools, the oxidation test methodology, and the sample characterization techniques. The fourth chapter will contain the results, and will therefore present the core findings and analysis of this thesis.

The core results of the thesis will be discussed in Chapter 5. Its results will be compared with others from the literature and will be put into perspective. The limits of the conclusions and of the research methodology will also be discussed.

Finally, the conclusion will summarize the key points of the thesis and offer suggestions to improve and further the research on AlOF protective coatings.

CHAPTER 2 LITERATURE REVIEW

2.1 Foreword

The following literature review presents the necessary information to interpret the results presented in chapter 4. It begins with a review of the titanium aluminides and their composition, structure, and properties, with a particular emphasis on the oxidation behavior of the TiAl. The existing solutions to protect TiAl against such oxidation are then presented. The halogen effect is discussed in more depth, as it is the solution used in this thesis. First, the theory behind the effect is discussed, followed by the usual implementation methods, with their advantages and drawback.

Then, sputtering is introduced. A very brief segment discusses the basics of plasma physics to lay the foundations for the physics of sputtering. The ion-target interactions, the design of the reactor, the advantages of the magnetron vs other cathodes, the choice of power supply, and the advantages and limitations of magnetron sputtering are all discussed.

After the review of basic sputtering, the concept of reactive sputtering is discussed. This section presents the advantages and drawbacks of reactive sputtering in opposition to its non-reactive counterpart. It also reviews the physics of reactive sputtering.

The final section of the literature reviews is about the chemistry of reactive O_2 and CF_4 plasma. Little literature exists on reactive sputtering using this specific gas mixture. Rather, most of the information about this type of discharge comes from research on plasma etching. This review will therefore use the knowledge of this field to discuss the interactions between oxygen and tetrafluoromethane, keeping in mind that sputtering is not initially taken into account in those publications.

2.2 Properties of γ-based titanium aluminides

Titanium aluminides are intermetallic compounds and as such, exhibit the characteristics of this special class of alloys. Their ordered structure and strong atomic bonds give them good mechanical properties like high elastic modulus, good structural stability, elevated melting temperatures, and good oxidation resistance. Due to the strength of the bonds and the low number of slip systems in the grains hindering the motion of dislocations, the mechanical properties remain strong at elevated temperature [14]. However, intermetallic compounds are known to be brittle and to have low toughness [9, 15, 16]. All those macrometric properties

are dependent on the microstructure and elemental composition of the alloy. The detailed physics and chemistry behind this relationship are quite complex and beyond the scope of this thesis. An overview is presented here.

2.2.1 Composition, phases, and microstructure of TiAl

The properties of TiAl are strongly dependent on its composition. To meet the needs of the industry, titanium aluminides have Al content between 38 and 50 at.% [7, 9]. In this range of composition and in the range of temperatures of possible applications (500 °C to 1100 °C), two phases (α_2 and γ) coexist in equilibrium, as seen in the Ti-Al phase diagram presented in figure 2.1.

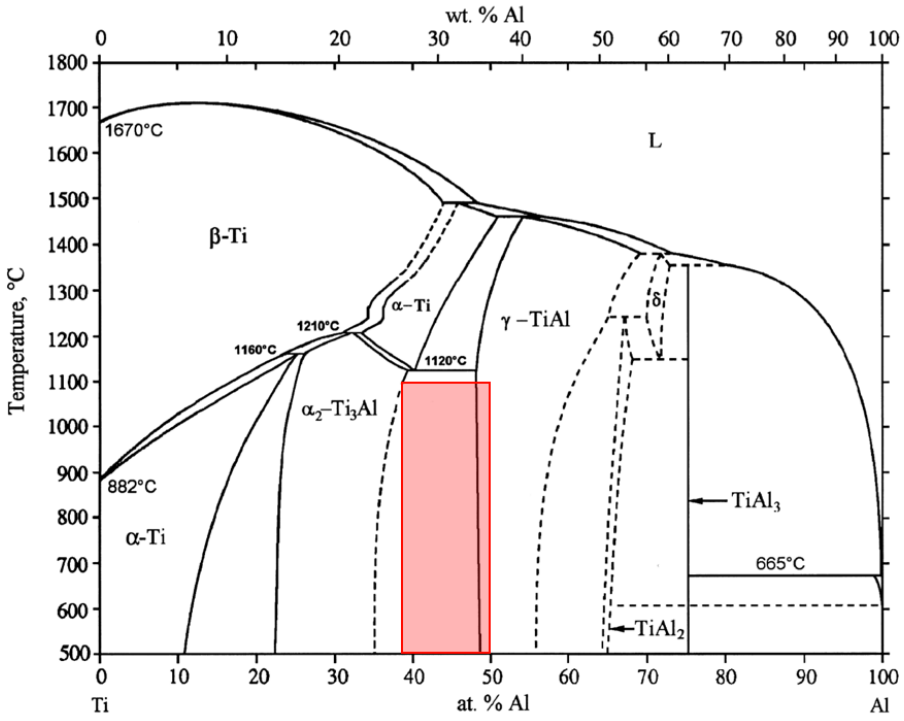

Figure 2.1 Ti-Al phase diagram. The compositions of industrial interest are highlighted. Reproduced from [1], with permission from Elsevier. Also, Intermetallics special credit, reprinted from [2] with permission from Elsevier. All rights reserved.

The γ and α_2-TiAl crystalline structures are presented in Figure 2.2. Alloys of technical significance usually contain both phases, in various proportions [7, 17]. The γ-TiAl have ordered face-centered tetragonal structure and have an Al content between 49 and 66 at.% [7]. The α_2 phase has a hexagonal close-packed structure [14]. Due to its elevated titanium content, the α_2 phase exhibits poor oxidation properties compared to the γ phase, which can

be an alumina former and generally exhibits fair oxidation resistance [7]. It is also lighter than α_2 (3.8 vs 4.2 g cm^{-3}). Both phases have relatively similar elastic moduli (176 MPa for γ and 145 MPa for α_2) [7]. One important difference between the two phases is their oxygen dissolution limit. The α_2 phase can dissolve up to 20 at.% of O, while the γ-TiAl can only dissolve 3 at.% [18].

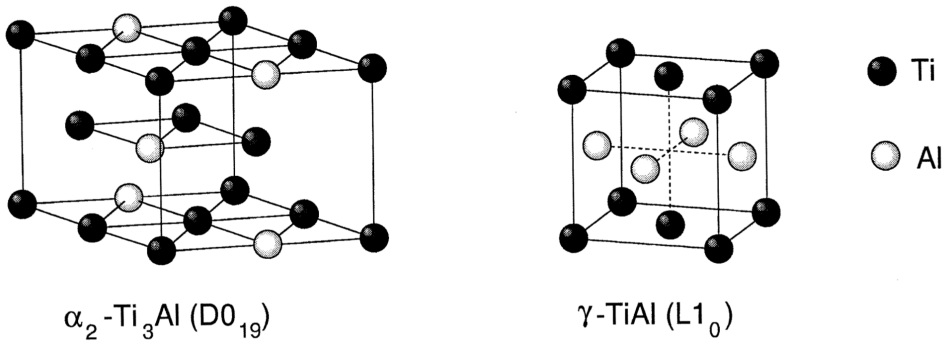

Figure 2.2 γ and α_2-TiAl crystalline structures. Reproduced from [1], with permission from Elsevier. All rights reserved.

The basic composition of the TiAl establishes which phase can develop in the alloys, which in turn impacts the mechanical and oxidative properties of the TiAl through its microstructure. In two-phased TiAl alloys, three types of microstructures can be observed, an equiaxed microstructure, a duplex structure, and a fully lamellar or near lamellar microstructure [9]. The equiaxed structure consists of single-phase γ grains. The lamellar structures consist of γ and α_2 lamellae. The duplex microstructure includes the two types of grains (γ equiaxed and γ/α_2 lamellae) [6, 9].

The lamellar TiAl exhibit the highest creep resistance, fracture toughness, and crack propagation resistance [6, 7, 9, 17]. The equiaxed γ grains are very brittle at room temperature but their ductility can be greatly improved if combined with lamellae grains to form duplex alloys. Indeed, duplex microstructures exhibit high tensile strength, ductility and longer fatigue life. Because of this enhanced ductility, the duplex microstructure is the most used in industry [6, 7, 9].

Many other microstructural parameters influence the mechanical properties of TiAl, like grain size, lamellae crystalline orientation and size. Those are all influenced by the manufacturing processes and available heat treatments. The addition of ternary and quaternary alloying elements can also have an effect on the microstructure by acting as stabilizers for some phases [6, 7, 9].

To refine the mechanical properties of TiAl beyond what pure Ti-Al metallurgy can offer, the addition of other elements is needed. They are added to improve ductility, strength, creep resistance, oxidation resistance, and to influence the microstructure by stabilizing certain phases and refining the grain size. The effect of those elements is summarized in Table 2.1.

Table 2.1 Effect of various elements on the microstructure and properties of TiAl

Property	Element
Ductility	Mn, Cr, Mo, B, V [7,9,17]
Strength	Nb, W, B, Ta [6,7,9]
Creep resistance	C, N, Si*, W*, Mo [6,7,17] *Causes embrittlement
Oxidation resistance	Nb, Ta, Zr, Mo, Cr, Mg, Y, Re, Si*, W* [7,17,19] *Causes embrittlement
α_2-phase stabilizer	O* [9,17] *Causes embrittlement
β-phase stabilizer	Cr, Nb, Mo, Ta [6]
Grain size refiner	B [6,7,17]

2.2.2 Mechanical properties of TiAl

The main mechanical properties of TiAl are listed in table 2.2, along with the corresponding properties of Ti-6Al-4V and Ni-based superalloys, also frequently used in the aerospace industry. Those properties serve as guidelines and vary from TiAl alloy to TiAl alloy depending on their composition and microstructure. This table should serve as a general guide rather than as an exhaustive list.

Table 2.2 Mechanical properties and melting temperature of cast TiAl, Ti-6Al-4V, and cast Ni superalloys.

Property	Cast γ-based TiAl	Ti-6Al-4V	Cast Ni superalloy
Density (g cm^{-3}) [7,9,14,20]	3.8 - 4.2	4.4-4.5	8.3-8.7
Yield strength (MPa) [14,20]	275-280	830	850
Ultimate yield strength (MPa) [14,20,21]	360-500	900	750 - 1400
Fracture toughness (MPa m$^{-0.5}$) [14,21]	115	55-115	100-150
Ductility (%) [14,20]	1-3	10	3-5
Elastic modulus (GPa) [14,20]	160-175	114	206
Poisson's ratio [20,22]	0.27	0.31	0.29
Melting temperature (°C) [7,14,22]	1440 to 1600	1600	1280

The advantages of TiAl, when compared to the other aerospace grade alloys, are clearly its density and elastic modulus. Its major drawback is its low ductility. An elongation of 1% after fracture is often cited as the minimal ductility required by material for airplane engines. An important amount of effort has been made in the past for the TiAls to simply meet this requirement [23]. However, when looking at specific mechanical properties (normalized to the density), TiAl properties approach or match those of the other alloys, as seen in table 2.3. Its specific elastic modulus is particularly high [9, 23].

Table 2.3 Specific properties of TiAl, Ti-6Al-4V and Ni-based superalloys

Property	Cast γ-based TiAl	Ti-6Al-4V	Cast Ni superalloy
Yield strength (MPa g^{-1} cm^3)	70-100	184	102
Ultimate yield strength (MPa g^{-1} cm^3)	90-103	200	120
Elastic modulus (GPa g^{-1} cm^3)	41-45	25	25

Those interesting mechanical properties warrant intense research and development around TiAl to overcome its drawbacks. However, despite expert microstructural and compositional engineering, TiAl remains very brittle. Furthermore, it is extremely difficult and costly to process titanium aluminides. This is perhaps their biggest flaw. Common issues during fabrication include non-homogeneous microstructure, in particular in large pieces, and high production costs [9, 23] The regular processing methods are extrusion (costly), forging (costly), casting (most cost-effective, allows for complex shapes, but requires precautions with the casting crucibles, inhomogeneity issues) and powder metallurgy (possible homogeneity issues, lower cost) [23]. Extrusion, forging and casting are used in industry, but all techniques are complex and suffer from high rejection rates [23].

2.2.3 Oxidation of γ-based TiAl

Beyond mechanical properties, the most relevant aspect of TiAl for this thesis is its oxidation behavior. As previously stated, the oxidation resistance of TiAl at temperatures greater than 750 °C is poor. The oxide that is produced at the surface of TiAl is composed of both Ti and Al oxide, is highly permeable to oxygen (which causes ongoing oxidation) and has poor mechanical properties (which results in heavy spalling) [24]. A scanning electron microscopy (SEM) micrograph showing the cross section of such an oxide scale is presented in Figure 2.3. The top of the oxide is composed of TiO_2. Just below, in the darkest shade of grey, is a continuous layer of Al_2O_3, followed by a mixed oxide scale of both TiO_2 and Al_2O_3. At the oxide/metal interface, diffusion of Nb at high temperature leads to the formation of Nb-rich nodules, in white in the figure.

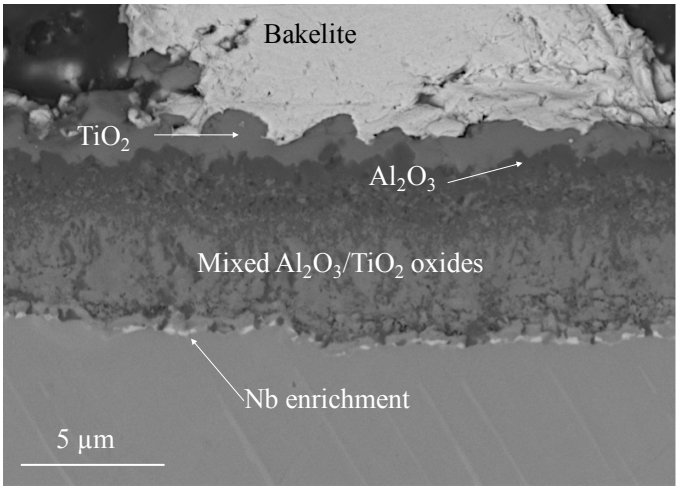

Figure 2.3 Cross-sectional view of oxidized TiAl 48-2-2 after 100h of oxidation in laboratory air at 850 °C.

The presence of TiO_2 in the oxide scale is problematic, as it is fast growing, porous, and brittle. However, the presence of slow-growing, stable and oxygen-impermeable oxides like Al_2O_3, Cr_2O_3, or SiO_2 is desirable [10]. Most of the protective solutions developed for TiAl aim at producing an alumina barrier, as it is quite compatible with the TiAl substrates. However, even with Al contents around 50 at.%, TiAls are not good alumina formers, i.e., they do not oxidize into pure alumina. It takes Al contents above 54 at.% (some even quote minimal content of 60 at.%) for TiAl to naturally form a continuous alumina scale, which does not correspond to the composition of the industrially significant TiAl alloys [10, 18, 25]. Therefore, it is necessary to improve TiAl 48-2-2 oxidation resistance by other means. In this section, the oxidation mechanisms of unprotected TiAl will be covered.

The oxidation behavior of TiAl can be explained by the extremely slow growth rate of aluminum oxide compared to titanium oxide, even though the activity of Ti and Al are similar [25]. A simple model to describe the growth and final structure of the oxide scale has been developed by Taniguchi *et al.* and Kerkare and Aswath [24, 26]. In the initial stage of oxidation, both Al and Ti are oxidized in the form of Al_2O_3 and TiO_2 islands. The rapid multidirectional growth of the rutile in comparison to that of the alumina ensures that the surface of the TiAl is quickly covered by titanium oxide. This explains why the upper part of the oxide scale consists of TiO_2 (see Figure 2.3. The fast diffusion of Ti toward the exterior, where the O_2partial pressure is high, leaves Kirkendall voids behind. The oxide scale is therefore porous and very permeable to oxygen [24, 26].

The conversion of Ti to its oxide depletes the subsurface in titanium, leaving behind an Al-rich zone that naturally oxidizes to Al_2O_3, as seen just below the TiO_2 first layer in Figure 2.3.

This Al enrichment is however not sufficient to build a solid Al_2O_3 oxygen barrier, and a mixed oxide scale builds up beneath the alumina layer. Since Ti diffuses faster than oxygen through TiO_2, the titanium diffuses outward and causes the TiO_2 to grow outward. On the other hand, the diffusion of Al in Al_2O_3 is much slower than that of oxygen, hence the inward growth of Al_2O_3. Therefore, in the mixed oxide zone, vertical channels of alumina and rutile can be seen side by side, each growing in their own opposite direction [24, 26–28]. Below this oxide, in the substrate, is a zone that is enriched in oxygen due to its constant inward diffusion. This oxygen enrichment is quite problematic because it embrittles the TiAl [24,29]. The oxygen affected zone extends between 25 and 50 μm deep in the TiAl [29].

The production of a pure and protective alumina scale is further complicated by the presence of nitrogen in the oxidation environment. The oxidation in normal air has indeed been shown to be worse than oxidation in pure oxygen, where the formation of pure alumina is easier [19, 30]. The reason behind the worsened oxidation in air is the formation of metal nitrides, coined as the "nitrogen effect". It is thought that the formation of TiN and Ti_2AlN, which get oxidized to TiO_2, competes with the oxidation of aluminum and hinders the formation of alumina in the early stages of oxidation [19, 28].

The oxidation kinetics of TiAl follow the law presented in Eq. 2.1

$$\Delta M^n = k_n t \tag{2.1}$$

where ΔM is the mass gain (usually in g cm^{-2}), t is the oxidation time (in hour), k_n is the oxidation rate constant (in g cm^{-2n} h^{-1}) and n is an exponent indicating the regime of oxidation. In the case where $n = 2$, the oxidation is limited by the diffusion of metals and oxygen through the oxide (diffusion-limited process) and is said to be parabolic. An $n = 1$ indicates linear oxidation, where oxidation is limited by chemical reaction rates, and not by the diffusion speed of species through the oxide scale [24, 28, 31]. Linear oxidation is usually seen when the oxide scale is porous or heavily cracked, allowing for direct contact between the metallic sample and the gaseous environment.

The oxidation rate constant depends exponentially on temperature, as seen in Eq. 2.2

$$k_n = k_0 e^{\frac{-Q}{RT}} \tag{2.2}$$

where k_0 is a constant (in g cm^{-2n} h^{-1}), Q is the oxidation activation energy (in kJ mol^{-1}, R is the ideal gas constant (in kJ mol^{-1} K^{-1}) and T is the oxidation temperature (in K). Activation energies and rate constants are useful to compare the oxidation behavior of dif-

ferent alloys, both among themselves and against the kinetics of pure TiO_2 and Al_2O_3. In general, oxide growth on TiAl follows oxidation kinetics between that of pure TiO_2 and pure Al_2O_3 [24, 28].

2.3 Oxidation protection of γ-based TiAl

Now that the oxidation behavior of TiAl has been discussed, it is important to understand the available solutions to prevent it. Those solutions are classified into two categories, namely alloying and surface engineering. As seen in Section 2.2, alloying with Nb, Ta, Zr, Mo, Cr, Mg, Y, Re, Si, and W can improve the oxidation resistance of the alloy [7, 17, 19]. Niobium is the most used of these additives and performs best when added in concentrations above 7 at.% [10]. In general, the role of those additives is to slow down the growth of the mixed oxide. This is achieved through i) the depletion of oxygen vacancies in TiO_2 which reduces oxygen diffusion, ii) the reduction of oxygen solubility in the TiAl to prevent internal oxidation, and iii) the increase of Al activity, which promotes the growth of a protective alumina scale [19]. This thesis will not cover alloying in more details, as its main focus is the deposition of thin films at the TiAl surface. The oxidation protection through surface engineering will now be discussed in more depth, with most of the emphasis put on the halogen effect.

2.3.1 Surface engineering for oxidation protection of TiAl: MCrAlY, aluminide and Cr-rich coatings

The careful alloying of TiAl can improve its oxidation resistance up to a temperature of 850 °C. To protect the TiAl parts at higher temperatures, and to reduce the constraints on the chemical composition of the TiAl, surface engineering is required [10]. In general, the surface modifications take the form of thin films or coatings, which promote the growth of stable and protective oxides like alumina, chromia or silica, with alumina being the most common [10]. Four categories of coatings can be enumerated, namely the MCrAlY coatings, the aluminide coatings, the Cr-rich coatings, and the halogenated coatings. The first three will be briefly discussed here, followed by an in-depth discussion on the halogen coatings.

The MCrAlY (where M is a metal like Ni or Ti), aluminides and Cr-rich coatings are usually deposited by physical vapor deposition (PVD) using sputtering, electron-beam evaporation or arc-PVD. They usually protect well the TiAl, sometimes at temperatures as high as 1000 °C [10]. A common issue with those coatings involves spallation due to a mismatch between the coefficient of thermal expansion (CTE) of the coating and the TiAl [6, 19, 32]. Interdiffusion between the substrate and the coating can also occur, inducing phase changes

which may be detrimental to the mechanical properties of the substrate [6, 10]. For example, the production of Laves phases ($Ti(CrAl)_2$) that are particularly brittle, although they are good alumina former [6, 32], can compromise the mechanical integrity of the TiAl. Ceramic coatings were also tested as an oxidation barrier. Nitride-based ceramics, like TiAlCrYN, often lead to the oxidation of the nitrides in TiO_2, which is not ultimately protective. CrAlN or CrAlYN offer long term oxidation protection up to 850 °C, but reactions between the titanium in the substrate and the nitrogen of the coatings degraded the ceramics and led to protection failures [10].

2.3.2 The halogen effect

The halogen effect is a very promising way to protect TiAl against oxidation and has shown effective protection at temperatures up to 1050 °C [10]. Its protective effect can be explained by the "gas transport model", which will be covered first, followed by a review of the existing processes using the halogen effect.

The gas transport model

In its simplest form, the gas transport model states that the presence of halogen forms metal halides that are oxidized at the surface of the TiAl. Here, fluorine is used as an example, but the model is valid for other halogens like Cl, Br, or I. The following reactions are at the base of the model [3, 33]:

$$2Al_{(s,TiAl)} + F_2 \longrightarrow 2\,AlF_{(g)} \tag{2.3}$$

$$4AlF_{(g)} + 3\,O_2 \longrightarrow 2\,Al_2O_{3(s,\text{oxide scale})} + 2\,F_2 \tag{2.4}$$

In other words, there is the creation of gaseous aluminum halides in or on the TiAl substrate, which then migrate via cracks and pores to the inner region of the oxide scale, where the oxygen partial pressure is high enough to initiate their oxidation [3]. The released fluorine can further react following two paths. The first is to form F_2. This F_2 can be recycled in reaction 2.3 to sustain the halogen effect over long periods of time. The second is for three fluorine atoms to react with the surrounding TiO_2 and convert it to TiF_3, releasing some O_2 for reaction 2.4 and consuming undesirable titanium oxide [33].

Instead of reaction 2.3, formation of the stoichiometric AlF_3 can also occur. However, it has been shown by thermodynamical calculation that only AlF will oxidize to Al_2O_3, and that the stoichiometric aluminum fluoride is not an important compound for the halogen effect [3].

Reactions 2.3 and 2.4 only show the production and oxidation of aluminum halides. However, titanium can also form halides and, eventually, detrimental TiO_2. Therefore, a crucial step in the production of a protective alumina scale is to ensure the *preferential* oxidation of the Al halides over the titanium halides. If the partial pressure of both types of halides is equal, they will oxidize at the same rate. One needs to maintain an imbalance in the partial pressures in favor of Al halides. This ideal partial pressure needs to be high enough to provide a sufficient flow of AlF to the oxide, without equating that of the Ti-halide. In other words, there is a "corridor" of Al-halides partial pressures within which a beneficial halogen effect can occur [3, 33].

To calculate this partial pressure corridor, one can use the flux $J_{\mathrm{Al}}^{\mathrm{ox}}$ of aluminum into the Al oxide (in mol cm^{-1} s^{-1}), which is proportional to the mass gain ΔM per unit time of the oxide scale. In the precise case of pure Al_2O_3, this relation becomes:

$$J_{\mathrm{Al}}^{\mathrm{ox}} = \frac{1}{24}\frac{d\Delta M}{dt} = \frac{1}{48}\left(\frac{k_n}{t}\right)^{1/2} \tag{2.5}$$

$J_{\mathrm{Al}}^{\mathrm{ox}}$ represents the minimal supply of Al that is required to enter the oxide scale in order to form Al_2O_3. This aluminum is transported to the oxide scale in the form of aluminum halide. The flux of Al (or halide) can also be calculated using the Hertz-Knudsen equation relating the flux of a gaseous species to its partial pressure P in Pa through its sticking coefficient α, its mass m in kg, the Boltzmann constant k_B in J^{-1}, the Avogadro constant N_A and the oxidation temperature T in K:

$$J = \frac{1}{N_A}\frac{\alpha P}{\sqrt{2\pi m k_B T}} \tag{2.6}$$

In the case of AlF equating those two fluxes gives the following equation for the minimal possible Al-halide pressure generating a pure Al_2O_3 scale [3, 18]:

$$P_{\mathrm{AlF}}^{\mathrm{min}} = \left(\frac{M_{\mathrm{AlF}} T k_n}{t}\right)^{\frac{1}{2}} \tag{2.7}$$

This minimal partial pressure is dependent on time, but also on the temperature of the oxidation. The minimal partial pressure of the parent halogen (here F) must be at least high enough to allow the $P_{\mathrm{AlF}}^{\mathrm{min}}$, the minimal partial pressure of AlF, to satisfy Eq.2.7.

The maximal partial pressure of the parent F is reached when the partial pressure of the TiF reaches $P_{\mathrm{AlF}}^{\mathrm{min}}$. Over this limit, it is titanium that is preferentially oxidized, and the halogen

effect becomes detrimental [3].

The relationship between $P_{\mathrm{AlF}}^{\mathrm{min}}$ and $P_{\mathrm{F}}^{\mathrm{min}}$ is usually calculated with software specialized in thermodynamic calculations, and will not be presented here. Figure 2.4 summarizes the reasoning presented above. Donchev *et al.* and Masset and Schutze have performed the calculations, allowing for a better understanding of this P_{F} corridor. The calculations were performed with chlorine instead of fluorine, at 900 °C and show the relationship between the partial pressure of different metal chlorides ($\mathrm{Me}_x\mathrm{Cl}_y$) as a function of the partial pressure of Cl_2. The minimal aluminum chloride partial pressure ($P_{\mathrm{AlCl}}^{\mathrm{min}}$, in black, horizontal), is calculated using Eq. 2.7, adapted for Cl. The minimal $P_{\mathrm{Cl}}^{\mathrm{min}}{}_2$ for a beneficial halogen effect occurs when the partial pressure of the AlCl equals the solution of Eq. 2.7. The maximal $P_{\mathrm{Cl}}^{\mathrm{mal}}{}_2$ occurs when the partial pressure of TiCl_3 equals that value [3, 18]. The corridor is thus defined.

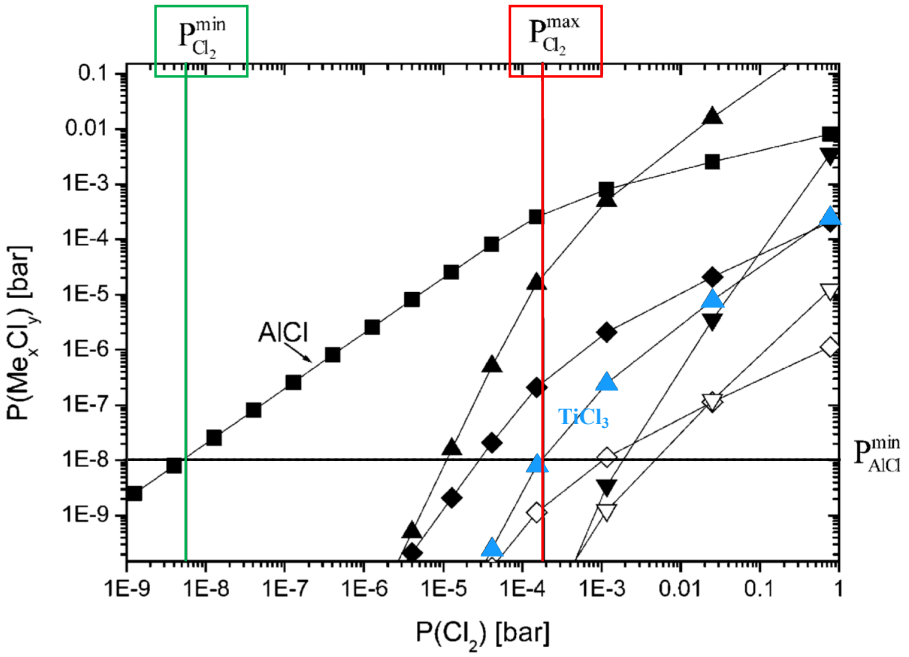

Figure 2.4 The partial pressures of different Al-chlorides and Ti-chlorides at a function of chloride partial pressure. Calculations performed at 1000 °C. The $P_{\mathrm{AlC}}^{\mathrm{min}}$, $P_{\mathrm{Cl}}^{\mathrm{min}}$ and $P_{\mathrm{Cl}}^{\mathrm{max}}$ are outlined in black, green and red respectively. Reproduced from [3], with permission from Elsevier. All rights reserved.

One can be interested in the nominal values defining the corridor, but also in its width, how it varies with oxidation temperature, and with the choice of halogen. It was found that of all halogens, fluorine has the widest corridor at temperatures of technological interest (700 °C and up [3, 18]. Furthermore, the corridor of fluorine broadens as temperature rises since

the aluminum fluorides are more stable than titanium fluorides at high temperatures [18]. This is advantageous from a process point of view, as it gives more flexibility to the surface engineer in terms of coating composition. Another major advantage of fluorine is that it performs well under cyclic oxidation, whereas Cl, the second most used halogen, offers little protection [34–36]. For these reasons, fluorine was chosen as a halogen for this thesis.

A drawback of using fluorine rather than another halogen is that fluorine can etch away the growing alumina. This may slow down the growth of the protective oxide scale in comparison to the case of chlorine. Also, the titanium halides are very stable and very volatile at low temperatures. Therefore, in the early stages of the oxidation, when the temperature is below 400 °C, a lot of fluorine evaporates in the form of titanium fluorides. For this reason, it is generally suggested to perform a short annealing at very high temperatures before using the fluorinated TiAl [18]. In general, as the temperature rises, the evaporation of Ti fluorides (as well as the evaporation of other sources of fluorine like F_2) is slowed by the appearance of a dense protective alumina scale which prohibits their evaporation [3]. In any case, the corridor of optimal fluorine partial pressure needs to be considered a theoretical tool rather than an absolute guide. Indeed, important fluorine loss mechanisms were not taken into account by the model. In addition to the evaporation of the titanium fluorides, not all of the produced aluminum fluorides will react to form alumina. Hence, a large initial supply of fluorine is needed so that the resulting partial pressure is sufficient.

Halogen effect implementation

The halogen effect is implemented using two groups of techniques, namely, ion implantation [33, 34, 36–38] and liquid or gas phase application [34, 36, 37].

The ion implantation technique is split into two sub-techniques: the beamline ion implantation (BLI^2) and the plasma immersion ion implantation (PI^3). The first requires the use of an ion accelerator, which is not practical, and only allows implantation on flat surfaces. The samples' shapes are limited and their edges are not well protected. However, assuming one has access to an accelerator, it allows good control of the dose and energy of the halogen ions, something that is not possible with the other techniques. It is therefore often used in fundamental studies. On the other hand, PI^3 can protect complex-shaped TiAl parts and has proven its ability to protect TiAl turbine blades [38]. In this procedure, a plasma is ignited around a heavily biased sample (tens of kV) in an atmosphere containing halogen. The halogen ions formed by the plasma are accelerated toward the sample by the bias. Regardless of the implantation method, one can control the energy of the incident ions, which affects the depth profile of the halogen concentration in the TiAl subsurface. Halogens implanted

too deep produce halides that cannot travel to the surface and get oxidized. The optimal implantation depth was found to be a few nm [33, 35]. Implantation is perhaps the only method that can deliver too high doses of halogens which exceed the optimal partial pressure corridor defined in Section 2.3.2. Other surface halogenation methods do not encounter this problem. Using Rutherford backscattering spectrometry and elastic recoil detection analysis on implanted TiAl, it was found that the optimal fluorine concentration implanted below the TiAl surface was around 60 at.%. This fluorine was implanted 50 nm to 200 nm below the TiAl surface [38]. It is difficult to establish whether a surface coating composed of 60 at.% would have the same protective effect as the implantation process, since the halogen is delivered to the surface of the alloy rather than in its subsurface. It is reasonable to assume that the surface coatings must be rather rich in fluorine to achieve a similar effect.

The liquid phase or gas phase applications include spraying, dipping, or vaporizing a halogenated compound onto TiAl like fluoropolymers or HF. The main advantage of this group of techniques is that it allows for the protection of complex shapes. Donchev and Schutze, for example, successfully protected pieces coming from turbocharger rotor by dipping the samples in a fluoropolymer [33, 36]. It is also simple, quick and inexpensive in comparison to the implantation methods. However, few studies exist on the optimization of the coatings process. No information is available on the type of fluorine compounds that were used, and on how their deposition was optimized with regards to parameters like F concentrations in the liquids or gases, time of treatment, the thickness of coatings, their effect on surface chemistry, etc.

A common observation made after the oxidation of protected TiAl is that there exists a zone below the surface that is depleted in aluminum. This depletion is explained by the important imbalance between the oxidation of Al and Ti, Al being consumed significantly out of the TiAl to form alumina [10, 39–42]. The TiAl depleted zone is usually constituted of α_2-Ti_3Al. Phase transformation of γ phase into the α_2 phase have been observed [41, 42]. This can modify the mechanical properties of the alloy. Since the α_2 phase can dissolve more oxygen than the γ phase, this can also accentuate the embrittlement of the surface due to oxygen dissolution.

A common observation made after the oxidation of protected TiAl halogen effect is that there exists a zone below the surface that is depleted in aluminum. This depletion is explained by the important imbalance between the oxidation of Al and Ti. The aluminum is rendered more active by the halogen effect and oxidizes at a higher rate than Ti. This increased formation of alumina pumps Al out of the TiAl substrate at a faster rate than Ti, which leaves an Al-poor region behind. The TiAl depleted zone is usually constituted of α_2-Ti_3Al.

Phases transformation of γ phase into the α_2 phase have been observed [41, 42]. This can modify the mechanical properties of the alloy. Since the α_2 phase can dissolve more oxygen than the γ phase, this can also accentuate the embrittlement of the surface due to oxygen dissolution [10, 39–42].

Both implantation and liquid phase treatment were shown to provide efficient and long-term protection against oxidation, with fluorine providing the best results. However, no work has been previously done on fluorination by sputtered films, a method that would allow control over fluorine concentrations in the films, their thickness, and their microstructure. The technique of sputtering will therefore be discussed next.

2.4 Plasma processes

2.4.1 Magnetron sputtering and reactive sputtering

In its simplest form, sputtering requires a vacuum chamber containing a cathode made of the material to be sputtered, a power supply, and a gas inlet. The pressure is lowered past one-thousandth of the atmospheric pressure, usually by a combination of turbo- and mechanical pumps. The gas is introduced to the chamber in a controlled fashion, keeping the pressure low. By applying a negative bias to the cathode, the gas in the chambers undergoes a dielectric breakdown, igniting a glow discharge. The positive ions created by this plasma are accelerated toward the cathode. The collision between the cathode and the incident ion displaces atoms in the cathode, sometimes ejecting some of them out of the solid. This ejection phenomenon is referred to as sputtering. The cathode, being the "target" of the plasma's ions, is referred to as the sputtering target. This section of the literature review will cover the basics of magnetron sputtering and reactive sputtering [4].

Magnetron sputtering

A schematic of a typical sputtering chamber is shown in Figure 2.5. In particular, this schematic shows a magnetron sputtering chamber, where there is a possibility to operate in reactive mode by introducing reactive gases in addition to the Ar working gas. In the reactor, a potential is applied to the magnetron and sputtering target, either in the form of a DC voltage, an RF, or pulsed signal. The electric field generated by this potential accelerates the electrons present randomly in the gas inside the chamber. The electrons collide with atoms in their path and ionize them if the acceleration provides them with an energy greater than the ionization threshold of their collision partner. The ions can then collide with the cathode itself, liberating more secondary electrons through those impacts. A secondary electron yield

can be defined as the number of expelled electrons per incident ion. The ever-growing number of electrons causes an electrical breakdown in the gas. In addition to ionization, the electronic collisions excite the atoms of the gas into higher electronic states, which can then relax and emit photons, producing the characteristic glow of plasmas. The secondary electrons help sustain the glow discharge, which is now in a steady state [4, 43].

The plasma is therefore composed of neutral species, excited species, and charged species (electrons and ions). The density of electrons and ions is assumed to be roughly equal. Hence, a plasma is often defined as quasi-neutral gas exhibiting a collective behavior, which comes from their collective interactions with electric fields. The ion density of sputtering plasmas like the one described in Figure 2.5 are generally very low (below 1%) and only increase when using high-power pulsed power supplies (High power impulse magnetron sputtering - HiPIMS) or inductively coupled plasmas [43, 44].

Nonetheless, the ions present in the plasma are sufficient to induce sputtering when they collide with the cathode. Indeed, as they get accelerated by the electric field of the cathode, some acquire enough energy to displace their atomic collision partner, which in turn displaces another atom in the target, which displaces another. Eventually, this linear cascade of impacts may eject one atom, whose trajectory is directed toward the target surface. The number of atoms ejected from the target per incident ion is called the sputtering yield. It is dependent on the average energy of the incident ions, on their mass and the mass of the target atoms, on the binding energy of the atoms in the target, and on the angle of incidence of the ion. Generally, in the setup of Figure 2.5, the sputtering yield is in the range of 0.1 to 3 atoms per ion, with incident ion energies in the range of a hundred eV [44].

The cathode of Figure 2.5 is composed of a magnetron. While not mandatory, there are advantages in using a magnetron rather than a simple electrode for sputtering. Indeed, the magnets inside the magnetron trap electrons in their magnetic field, inducing a gyration motion. The traveled path of a single electron before its absorption on surfaces is therefore increased dramatically, because the number of possible (ionizing) collisions increases with the travelled distance. Hence, the use of a magnetic field increases the ion production per electron, which increases the sputtering rate. It also allows the use of lower pressure in the reactor, since high ionization rates can be achieved with fewer collisions. Lowering pressure increases the mean free path of the species in the plasma, i.e. the ions can travel further without collisions. Therefore, once accelerated by a potential, they keep this kinetic energy instead of losing it to collisions, which is useful to engineer some properties of the sputtered thin film [4]. The details of film engineering with energetic ions will not be discussed here and is in itself a very interesting, complex and useful area of the sputtering science. For

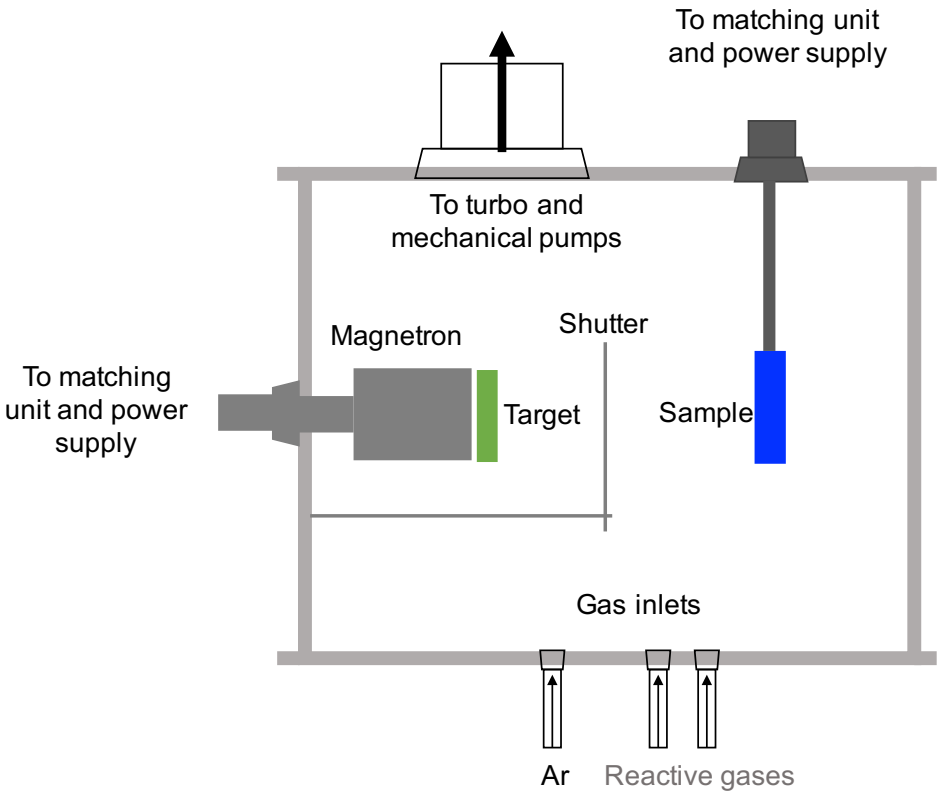

Figure 2.5 A simplified magnetron sputtering reactor.

now, it suffices to say that magnetron sputtering greatly improves the sputtering rates, the deposition rates and the quality of the resulting coatings.

The magnetron's magnets are often "unbalanced", which means that the magnetic field lines do not close on themselves. Rather, they extend toward the substrate holder, forcing the electrons to go outwards. This enhanced flux of electrons (and ions) near the sample increases the energy of the incident ions on the growing film [4].

While magnetrons can be powered by a variety of power supplies, this project required the use of an RF power supply, as it is the type of power supply that is best suited for reactive sputtering. Indeed, the buildup of oxide on the surface of the cathode makes it impossible to power the magnetron with a DC potential, which would only accumulate charge. Pulsed power supplies have a tendency to create micro-arcs when used with an oxidized target, which causes surface defects on the growing film. The use of an alternating RF potential circumvents those problems and allows for the sputtering of dielectrics [4].

From an experimental point of view, the following parameters can be controlled during sputtering: i) the type of power supply, the power (or voltage) applied to the magnetron, ii) the

gas pressure in the system, iii) the nature and the flow of gas, iv) the bias on the sample substrate. In general, RF sputtering is performed at a set power, and the cathode voltage is adjusted to maintain that power. The opposite is however also possible. Additional features like a heating element or a rotating substrate holder can be used to perfect the deposition.

Reactive magnetron sputtering

Apart from metals, which are easily sputtered, there is a technological need to sputter dielectric materials like oxides, nitrides, or carbides. It is possible to sputter those compounds using a dielectric target, but they are usually fragile and the stoichiometry of the sputtered film is that of the target, with little possibility to adjust it. For these reasons, reactive sputtering has come along, allowing the use of metallic sputtering targets while offering more control over the composition of the thin film [4,45]. It requires that a reactive gas be injected to the reactor along with the noble working gas. This gas reacts with the sputtered material to form a compound film on the substrate. The arrival of reactive gas strongly modifies the state of the target and affects the behavior of the whole plasma. This section will summarize those effects and their impact on the sputtered film. For simplicity, it will be assumed that the reactive gas is oxygen, but the following will also apply to other reactive gases.

The presence of oxygen in the reactor oxidizes all accessible metallic surfaces, including the sputtered metal, the metallic target, and the reactor's walls. The target oxidation is called "poisoning". Target poisoning reduces its sputtering yield because the binding energy of atoms in an oxide (or other ceramic compounds) is greater than that of the metal. This reduction in sputtering yield leads to a reduction in the deposition rate, which is problematic for most technological applications. Furthermore, poisoning modifies the secondary electron yield of the target, which is reduced in the case of oxides, but can in general increase or decrease depending on the compound's electron binding energy. The variation of secondary electron yield has a direct impact on the electron and ion densities in the plasma [4].

Ideally, the layer of oxide on the target would remain thin and would be sputtered away as it builds up, so that the plasma is the least perturbed by the injection of reactive gas. The level of poisoning is controlled experimentally by the flow of reactive gas entering the system, and by the pumping speed. The effect of this gas flow on the pressure in the reactor is shown in Figure 2.6 and is quite useful to understand the mechanisms behind poisoning.

When first adding oxygen to the gas mixture (0 to 2.25 sccm in Figure 2.6), the pressure almost doesn't vary. This is due to capture of the reactive gas on the metallic surfaces. Indeed, in addition to the actual turbo and mechanical pumps of the reactor, its metallic components (including the surface of the target and sputtered metal) act as getters for the

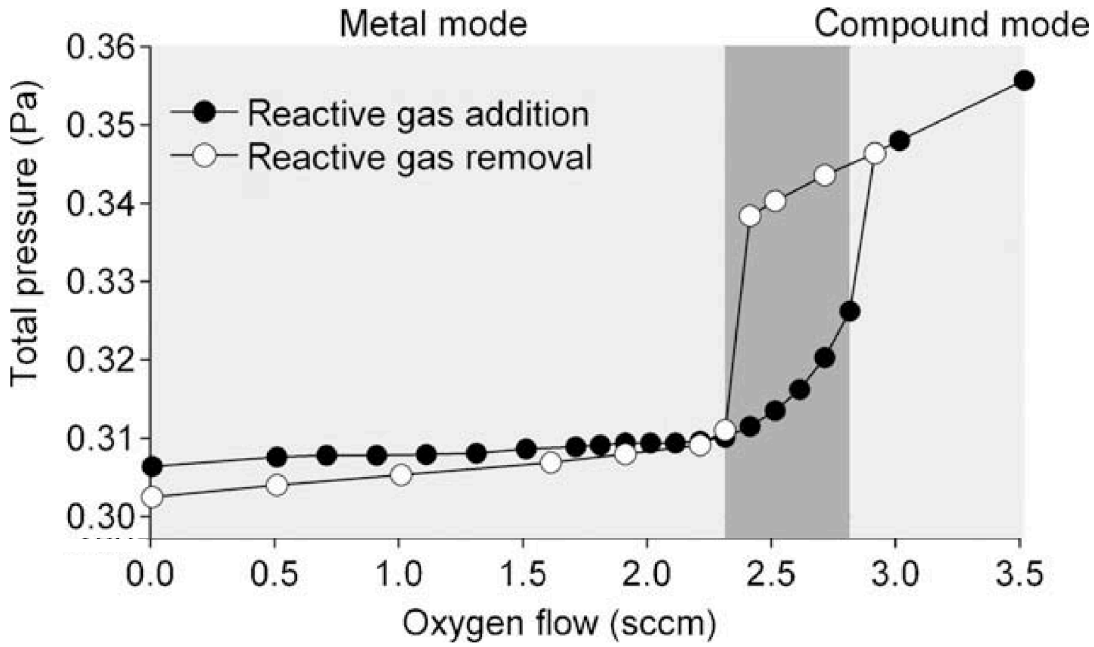

Figure 2.6 The total pressure in the reactor as a function of oxygen flow, which exemplifies the hysteresis of the system. Reproduced from [4], with permission from Elsevier. All rights reserved.

oxygen. This is considered a "second pump" of the system. This pump continues to collect oxygen until it saturates. This occurs when the reactor's walls are oxidized, and when the oxygen flow is too high for the target to sputter-clean itself. When that occurs, the target is not a source of sputtered metal, but a source of oxide, which cannot act as a getter like the metal did. The "second pump" is saturated and becomes inactive, hence the rise in the total pressure in the system. After this rise (at around 2.75 sccm of O_2 in Figure 2.6), the pressure increases linearly with the reactive gas flow [4].

Once the oxygen supply is removed, the oxide on the target is eventually sputtered away, and the target becomes once again metallic. However, as the sputter yield of oxides is very low, a delay exists between the moment where the oxygen flow is interrupted and where the target becomes metallic. The delay, or hysteresis, is highlighted in dark grey in Figure 2.6, between 2.3 and 2.75 sccm of O_2. This hysteresis is also seen in other measurable quantities, like the cathode bias in RF sputtering, which decreases significantly once the target is poisoned.

The films produced in the metallic mode are usually sub-stoichiometric. On the other hand, the deposition rates in the poisoned mode are too low to be of technological interest. The ideal gas flux for efficient deposition of quality films is as close as possible to the onset of poisoning. However, because of the very steep transition between the metallic and poisoned

mode, it is difficult to operate a stable discharge at that oxygen flow. In addition, the presence of hysteresis when going back and forth between the two modes makes the process even more difficult to control. Operating a stable reactive sputtering discharge to produce high-quality, reproducible thin films is quite an art. Several technologies have been developed to assist such depositions, like automated feedback loops that adjust the reactive gas flows to maintain the pressure, the cathode voltage, the current or any other chosen discharge parameter constant [4].

In addition to the target's chemical state, the gas phase chemistry of reactive plasma is quite important. This topic will be the focus of the next section, which will cover the specifics of O_2 and CF_4 reactive plasmas.

2.4.2 CF_4 and O_2 etching plasmas

The chemistry of CF_4 plasma has been studied most by the etching community. At first, it was extensively used to etch Si and SiO_2 for microelectronic applications. It was rapidly discovered that the addition of oxygen to CF_4 improved etch rates [13, 46, 47]. The interactions between oxygen and the fluorocarbons are therefore well discussed, and as such, plasma etching chemistry will serve as the stepping stone for the understanding of reactive $Ar/O_2/CF_4$ sputtering plasmas.

Pure CF_4 plasma

At the base of the etching process is electron impact dissociation of CF_4, producing numerous reactive species in the gas phase, which partake in etching by forming volatile products at the surface of a specimen. Indeed, the CF_4 molecule is not very reactive itself and does not produce a stable ion [47, 48]. It is, however, a good source of $CF_{x=1,2,3}$ fragments, either ionized, exited, or in their ground state. Even more important, it is a good source of atomic fluorine, which is very reactive and at the core of the etching process [13, 48, 49].

CF_4 dissociates into neutrals and ions via electron impact dissociation, according to the following main reactions and their specific energy thresholds [13,32,47,48,50,51]. In addition to producing fluorocarbon fragments, those reactions produce atomic fluorine, which is the most active of the etching species. Reaction 2.9, which produces a negative fluorine ion, is followed by electron recombination to form atomic fluorine.

$$CF_4 + e \xrightarrow{12.5\ eV} CF_3 + F + e \tag{2.8}$$

$$CF_4 + e \xrightarrow{5\ to\ 6\ eV} CF_3 + F^- \tag{2.9}$$

$$CF_4 + e \xrightarrow{9.5\ eV} CF_2 + 2\,F \tag{2.10}$$

$$CF_4 + e \xrightarrow{15.6\ to\ 16.2\ eV} {CF_3}^+ + F + 2\,e \tag{2.11}$$

The dissociation of CF_4 leads to the formation of CF_2 twice as often as CF_3 [32, 50, 52]. The formation of the smaller CF fragment is of lesser importance and is often neglected. The formation of ions, mainly via reaction 2.11, occurs in high energy regimes (electron impact energies greater than 35 eV). In a low energy regime, CF_4 mainly dissociates into neutral CF_2 and CF_3 [48].

In addition to dissociative reactions, important recombination reactions occur readily in the gas phase and deplete the plasma of key molecules. The most important are

$$CF_3 + F + M \longrightarrow CF_4 + M \tag{2.12}$$

$$CF_3 + F^- \longrightarrow CF_4 + e \tag{2.13}$$

$$F + F + M \longrightarrow F_2 + M \tag{2.14}$$

$$CF_3 + CF_3 + M \longrightarrow C_2F_6 + M \tag{2.15}$$

where M is a third body, often a wall or a surface. The recombination of F and CF_3 is the dominating loss reaction [52].

2.4.3 Addition of O_2 to CF_4 discharges

The addition of small amounts of oxygen to fluorocarbon discharges is known to increase both the etch rate and the concentration of fluorine atoms in the gas phase [13, 46, 47]. The addition of O_2 to the gas mixture creates carbonyl fluorides and difluoride (COF and COF_2, as well as carbon mono- and dioxides that are absent from the pure CF_4 discharges. The fluorine enrichment operates via [13, 53]

$$CF_3 + O_2 \longrightarrow COF_2 + OF \tag{2.16}$$

$$CF_3 + O \longrightarrow COF_2 + F \tag{2.17}$$

$$CF_3 + O_2 + M \longrightarrow CF_3O_2 + M \tag{2.18}$$

The additional fluorine is either directly produced (like in reaction 2.17), or is liberated during the subsequent reaction of OF via [13]:

$$OF + CF_3 \longrightarrow COF_2 + 2\,F \tag{2.19}$$

Those reactions occur alongside the usual CF_4 dissociation reactions. In time, the COF_2 dissociates and reacts further to form COF, CO_2, and CO [32].

It is important to note that the role of oxygen is twofold. First, it directly generates F trough reactions 2.16 to 2.19. Second, by reaction with CF_3, it removes important recombination pathways for fluorine and CF_3. Indeed, the consumption of CF_3 via its oxidation suppresses recombination opportunities by reactions 2.12, 2.13, and 2.15 [13]. The role of CF_3 is therefore established as being both a source of F, through its oxidation, and a sink of F through recombination. The importance of each role is determined by the relative availability of either F for recombination or oxygen for oxidation [32].

The relative availability of F and O also impacts the role of the numerous CF_2 fragments produced by the discharge. At high oxygen flows, CF_2 reacts primarily with oxygen, rather than recombining with F to form CF_3:

$$CF_2 + O \longrightarrow COF + F \tag{2.20}$$

High oxygen concentration ensures rapid subsequent oxidation of COF into CO_2. If the plasma is oxygen-poor, CF_2 will react with F, producing CF_3 by heterogeneous recombination [32].

To conclude, the production of atomic fluorine is therefore ensured by CF_4, CF_3, and CF_2. The careful balance between fluorine production and recombination dictates the composition of the plasma. The reactions and chemistry outlined in this section pertain to etching, but can also be transposed to sputtering. However, continuous supply of sputtered metal is expected to shift the balance toward increased recombination, as more third bodies become available both in the gas phase and on all of the surfaces of the reactor.

CHAPTER 3 METHODOLOGY

This section describes the various laboratory manipulations and techniques used to prepare samples, to deposit coatings, to monitor the plasma, oxidize the samples, and characterize them.

3.1 Sample preparation

The TiAl 4822 samples were first cut into small coupons of approximately 80x12x3 mm and pierced to allow their installation in the reactor according to Figure 3.1. The TiAl samples were then ground with SiC grinding paper with grit number starting at 320 and ending at 2000. The edges were rounded and ground as well to avoid coating delamination and oxide scale spallation due to stress concentration at sharp edges. The final polish was obtained by polishing the flat sides only with a 6 μm diamond paste and an oxide polishing suspension (OP-S) of silica until a mirror finish was attained.

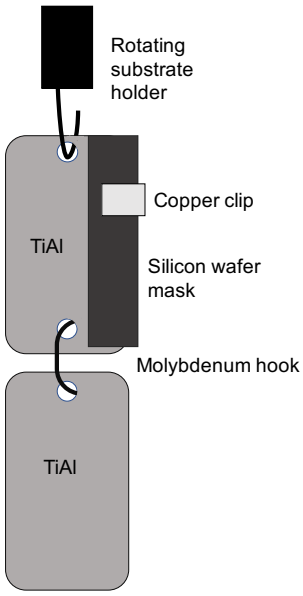

Figure 3.1 A schematic of the sample installation, showing two TiAl samples linked by a Mo wire, and hooked to a rotating substrate holder. The top sample was half-covered by a piece of Si wafer.

Prior to installation in the plasma reactor, the TiAl were cleaned using ultrasonic cleaning in acetone and isopropanol for 15 minutes each. They were then dried with compressed air and installed in the reactor.

The samples were put in pairs in the reactor, linked by a chain like in Figure 3.1. To monitor the deposition rates, a silicon mask was installed on one half of the top sample, held with a copped clip. The other half served for coating analysis. The bottom sample was kept for oxidation tests and was kept bare so that its whole surface can be coated.

It is common to sputter-clean samples in an Ar plasma prior to deposition, in order to remove any last contaminants from their surface and maximize adhesion of the coating. It was found that the procedure was etching away the Si wafer and Mo, and contaminating the surface with those elements. Because it was primordial to deposit coatings of the same thickness for comparison purposes, it was decided to keep the Si wafer and skip the Ar cleaning. It will be possible to return to this step in the future, once a successful coating recipe has been developed.

3.2 Sputtering

3.2.1 The sputtering reactor

The sputtering reactor used for the project is similar to the one in Figure 2.5. The stainless-steel reactor had an approximate volume of 20 L and was pumped by a turbo pump backed by a mechanical pump. A 2-inch aluminum target was mounted on the water-cooled, unbalanced magnetron. The power was supplied by an RF generator operating at a frequency of 13.56 MHz. A matching unit was used between the output of the power supply and the magnetron to ensure a proper impedance match between the two components.

The substrate holder was rotated by an external electrical motor at a speed of 10 rotations per minutes. This allowed all sides of the samples to be coated. The samples were held 12 cm away from the magnetron and were left at floating potential.

The base pressure of the system was at less than 4×10^{-3} Pa, as measured by a full range cold cathode pressure gauge.The pressure during depositions was measured by a Baratron manometer and was kept constant at 20 mTorr by the actuation of a butterfly valve at the entrance of the turbopump. The system was equipped with three gas lines entering the reactor behind the magnetron. The gases used were Ar, O_2 and CF_4. The CF_4 line was heated during depositions to avoid flow fluctuation due to condensation of the gas in the pipe.

3.2.2 The deposition protocol

The first step of the sputtering process was to sputter clean the target, to ensure that traces of previous poisoning were removed before proceeding with the deposition. The cleaning was performed with the shutter closed, at 200 W of RF power, 20 mTorr of pressure in the reactor, high fluxes of argon (60 sccm), for a duration of 20 minutes. This cleaning of the sputtering target was not followed by an Ar cleaning of the sample, as discussed in Section 3.1.

The second step was to proceed with the deposition of an aluminum bond coat, to maximize the adhesion of the AlOF coating. The 100 nm thick bond coats were sputtered on rotating samples in an Ar atmosphere at 200 W, 20 mTorr, using an Ar flow of 15 sccm.

Finally, the AlOF coatings were deposited. The reactive gases (O_2, various flows from 0.5 to 10 sccm, and CF_4, 8 sccm) were introduced into the chamber together while the shutter was closed to protect the samples. After two minutes, after which the plasma had reached a new equilibrium, the shutter was opened and the deposition began. Again, the samples were rotating. Once the desired deposition time was reached, the power and gas flux were stopped, and the sample was left to cool for 10 minutes before being collected.

3.3 Mass spectrometry

Mass spectrometry (MS) was used to gain insights on the chemistry of Ar, O_2 and CF_4 plasma. MS is a technique that determines the masses of the different constituents of a gas mixture. It consists of an ionizing cell, a mass analyzer, and a detector, and can include an energy analyzer to determine the energy of the gas constituents as well. The spectrometer can perform in "residual gas analysis" (RGA) mode, where neutral particles are detected, and in ion detection mode. In the case of this thesis, an EQP-1000 mass spectrometer by Hiden Analytical equipped with an energy analyzer and a quadrupole mass filter was operated in RGA mode [54].

In RGA mode, the gas in the plasma reactor diffuses into the spectrometer's ionization chamber through a small orifice at the entrance of the spectrometer. There, it is ionized by electron impact. The ions travel through the energy analyzer (not used in this study) and finally through the four rods of the mass analyzer. An RF potential is applied to those rods in pairs, each pair having a different DC voltage offset. For a given offset ratio, only an ion of a certain mass-to-charge ratio will oscillate in the RF electric field without colliding with the rods, and eventually reach the final detector. By sweeping the potentials on the rods, and counting how many ions successfully cross the quadrupole, one can obtain a mass spectra i.e., counts as a function of mass/charge of the ion [54].

From an experimental point of view, one can control the energy of the electrons in the ionizer, and the current it uses. In general, the electron energy is set to 70 eV, which is above the ionization energy threshold of most atoms and compounds, so that all of them can be detected. The rest of the spectrometer's parameters, mostly potentials applied to different filters (like the mass analyzer) and various electronic lenses, are generally calibrated once and not varied during experiments.

When operating in RGA mode, is important to distinguish between the products created in the ionization chamber and in the plasma reactor. Indeed, the final mass spectrum does not differentiate between the two types of species. For example, one could be interested in the amount of neutral CF_3 produced during reactive sputtering in CF_4. One can safely assume that some CF_3 will be produced in the plasma and will diffuse into the spectrometer, be ionized to ${CF_3}^+$ in the ionizer, and be detected. However, a CF_4 molecule diffusing into the spectrometer can undergo electron impact dissociation and produce a ${CF_3}^+$ ion that will also be detected in the same manner as the previous ion. However, the ion produced by the latter scenario does not come from the plasma and is not representative if the plasma chemistry. Hence, it is important to obtain mass spectra while the plasma is both on and off, to decouple the reactions occurring in the plasma and in the ionizer. In the same line of thought, spectra of the empty plasma reactor were acquired to characterize the residual gases inside as well as in the mass spectrometer itself.

The MS measurements were done on a different reactor than the sputtering reactor because it was impossible to install the spectrometer on the latter, nor was it possible to modify the MS reactor to accommodate a rotating sample holder, which is mandatory for depositions on samples dedicated to mass gain-sensitive experiments. The MS reactor was however very similar to the sputtering reactor. The 20 L stainless steel chamber was equipped with a 2-inch unbalanced magnetron powered by an RF power source. The system was pumped by a turbo and a mechanical pump to pressures below 4×10^{-3} Pa. The mass spectrometer was also pumped by its own turbo and mechanical pumps, to a pressure below 2.7×10^{-5} Torr. The orifice joining the mass spectrometer to the reactor had a diameter of 150 μm and was located 15 cm away from the magnetron.

3.4 Oxidation tests

Once fully coated, the TiAl samples' surface areas were calculated. The length of all the edges of a sample was measured using a digital Vernier caliper. The total area was calculated by summing the individual areas of faces, assuming that they were trapezes in order to account for the angles created by polishing and cutting the samples. Their initial mass was measured

using a micro-balance precise to 10 μg.

The samples were then oxidized in laboratory air in a conventional oven for 50 hours. They were inserted into the oven once it had reached the appropriate temperature. This was to ensure that the sample heated quickly past the temperature range of maximal stability for the titanium fluoride (400 °C and less, see Section 2.3.2). The samples were then weighed after 2, 4, 6, 15, 25 and 50 hours of oxidation. They were taken out of the oven, cooled during 5 minutes in ambient air, re-weighed, and put back in the oven. The frequent thermal shocks occasioned by this methodology simulate a rather severe working environment.

The mass gains were calculated by dividing the measured mass of a sample by its surface area and subtracting its mass per area at time zero.

3.5 Sample characterization

The characterization of samples can be divided into that of physical properties, like the morphology or the crystallinity of the samples, and that of chemical composition. Both will be described below.

3.5.1 Physical characterization

Scanning electron microscopy

Scanning electron microscopy (SEM) is a type of microscopy that uses electrons to image a surface, rather than photons in optical microscopy. The high energy of the electron beam (1 to 30 keV) allows for high-resolution imaging (resolution is inversely proportional to the incident particle's energy). The interaction between the electrons and the scanned sample produces secondary electrons, backscattered electrons, and x-rays. The secondary electrons are weakly-bound valence or conduction band electrons that are ejected from the sample by the incident beam. They have small kinetics energies (typically less than 15 eV), and as such, cannot travel through thick materials. Therefore, they come from the very surface of the samples (first nanometers), providing nm-scale information about its topology [55].

Backscattered electrons are electrons from the beam that elastically collide with the sample's atoms and get reflected back. Heavy atoms in the sample backscatter more electrons than light atoms and appear brighter. Operating an SEM in backscattering mode therefore provides chemical contrast. The energy of backscattered electrons is much greater than that of secondary electrons. They therefore come from deeper in the sample, which makes this mode less sensitive to surface topology than the secondary electron mode. However, tilted

surfaces have greater backscattering yield and can appear brighter than flat ones, providing this mode with some sensitivity to topography [55].

The SEM images taken for this thesis were acquired on a JEOL JSM-7600F field emission microscope. The secondary electron mode was used for surface imaging, while samples' cross-sections were imaged using backscattered electrons for optimal chemical contrast. The acceleration voltage of the electron beam was of 10 kV, working in high current mode. Surface preparation involved sonication for the surface imaging, and bakelite mounting followed by polishing (same procedure as in Section 3.1) and gold sputtering for the cross-sections.

3.5.2 Chemical composition

Rutherford backscattering spectroscopy

Rutherford backscattering spectrometry (RBS) is a useful technique to quantify the chemical composition of a sample and to establish depth profiles of that composition. A high energy ion beam is focused on the surface of the sample, and the energy of the backscattered ions is measured. It is assumed that the collisions are elastic [56].

This energy depends on both the composition of the atom struck by the beam and his depth below the sample's surface. By recording the energy of the backscattered ions, a spectrum of the number of counts at each energy can be obtained. To interpret the spectrum, it is compared to theoretical spectra produced by models. The calculations use collisional cross-sections to calculate the theoretical energies of backscattered ions stricking a theoretical sample, whose composition and structure is adjusted until a good fit with the experimental data is achieved [56].

In this thesis, the RBS measurements were performed at the Université de Montréal, in their Tandetron accelerator. A helium ion beam of 3.645 MeV was used to probe the surface of coated TiAl. The SIMNRA software was used to model and fit the experimental data.

Energy dispersive x-ray spectroscopy

Energy dispersive x-ray spectroscopy it a technique used to determine the chemical composition of a sample in a quantitative way. It is used inside an SEM, where the electron beam is used to produce the x-rays. Instead of ejecting an outer shell electron like the secondary electrons, the incident beam sometimes ejects a core electron, leaving behind an empty energy level that is rapidly filled by a higher energy electron relaxing. This transition to a lower energy level releases an x-ray, whose energy is characteristic of the target atom. By record-

ing this energy, one can identify and quantify the composition of the sample. By scanning the beam, line profiles and maps of compositions can be obtained, making EDS a versatile tool [55]. The EDS used in this thesis was an X-MaxN detector from Oxford Instruments. The AZtec software was used to acquire and analyze the data.

CHAPTER 4 RESULTS

4.1 Foreword

This section presents the main results of the thesis. It is separated into three themes. It first makes an analysis of the parametric space of the plasma sputtering condition and evaluates the chemical composition of the plasma at each point. More specifically, the investigated parameters are sputtering power and oxygen gas flow, while working at constant pressure and maximal CF_4 flow, to maximize fluorination. This is followed by the fabrication of AlOF coatings at different sputtering conditions, to evaluate the relationship between the chemistry of the plasma and the chemistry of the coatings. Finally, some key AlOF coatings are tested during isothermal oxidation tests at 875 °C. The oxidation kinetics of the best coatings are discussed and compared against those of unprotected TiAl and of other halogen treatments. A full description of the plasma dynamics, its influence on coatings' nature and their oxidation performances can therefore be provided.

4.2 Results

4.2.1 Mass Spectrometry

Identification of species

In the first part of this work, we attempted to identify the neutral species participating in the reactive sputtering $CF_4/Ar/O_2$ plasma using MS. Starting with a simple Ar sputtering plasma, the reactive gases were added one at a time and then together to the reactor, to identify the origin of molecules. To distinguish the molecular fragments produced by the plasma from those produced in the ionization chamber of the spectrometer, mass spectra were acquired before and after igniting the plasma. When the plasma was turned on or off, or when an experimental parameter was modified, the plasma was allowed to equilibrate for two minutes before a measurement was taken. The differential spectra, obtained by subtracting the signal of the ignited plasma from that of the extinguished one, are presented in Figure 4.1. The reactor pressure was maintained at 20 mTorr, with a constant Ar flow of 15 sccm, and O_2 and CF_4 flows of 5 sccm each when required. The intensities were normalized to the Ar 40 intensity, similar to all subsequent MS spectra, to eliminate any time-varying sensitivity of the spectrometer.

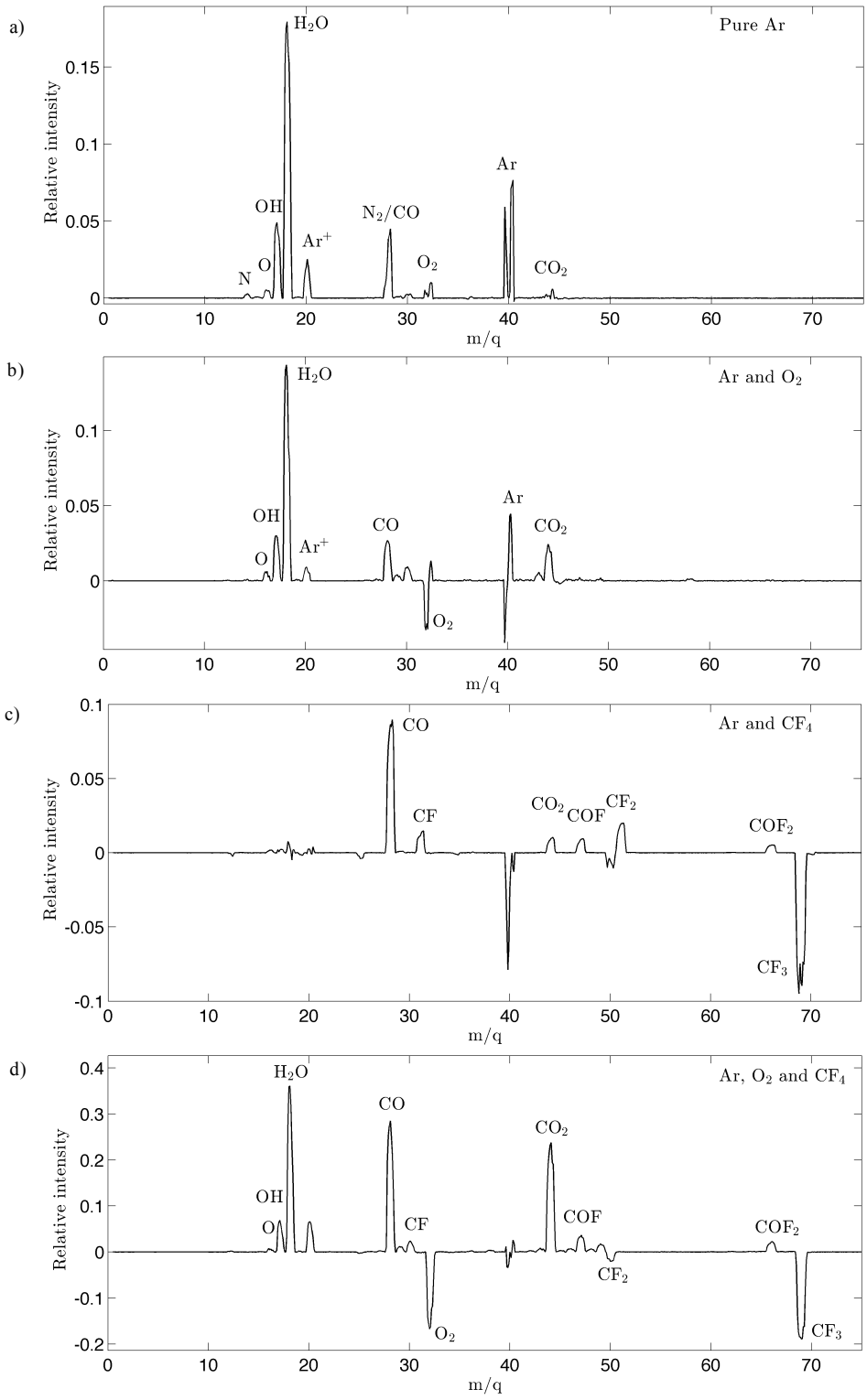

Figure 4.1 Differential mass spectra of aluminum sputtering plasmas generated using 150 W RF power (when plasma was ignited) with a) 15 sccm of Ar, b) 15 sccm Ar and 5 sccm O_2 c) 15 sccm Ar and 5 sccm CF_4, d) 15 sccm Ar, 5 sccm O_2 and 5 sccm CF_4. The total pressure was kept constant at 20 mTorr. Intensities are normalized to Ar 40.

In Figure 4.1 a), the absence of negative peaks indicates that the plasma contributes to the presence of all detected species, most of which are desorbing contaminants like water (18 amu/q), N (14 amu/q), O (16 amu/q) and O_2 (32 amu/q), OH (17 amu/q), N_2 and CO (28 amu/q), and CO_2 (44 amu/q). The Ar signal (40 amu/q) is well visible when looking at the spectra individually, but it is in this case distorted by the subtraction of spectra. On the other hand, Ar+ (20 amu/q) is clearly a product of plasma ignition. The sputtered aluminum is absent from this spectrum, as well as from the others. Indeed, sputtered metal atoms have more kinetic energy than the working gases, which prevents the aluminum from passing through the spectrometer's energy filters.

In Figure 4.1 b), the addition of oxygen stimulates the formation of CO2. It is interesting to note that the reactor is poorer in molecular oxygen when the plasma is on, indicating that it strongly reacts with residual C to form CO_2 and that it is heavily dissociated to form atomic O. The other contaminants like H_2O, OH and CO observed in the pure Ar plasma remain, with the exception of N.

The addition of CF_4 in Figure 4.1 c) brings CF_4 fragments in the gas phase, with CF_3 (69 amu/) being the most abundant, followed by CF_2 (50 amu/q), and CF (amu/q). CF_4 itself cannot be identified by MS since it has no stable positive ions [48]. Atomic F is identifiable on the individual spectra, but it disappears from the differential spectrum as its intensity is similar with and without plasma. COF and COF_2 are produced by the plasma, through the reaction of carbonated fragments with residual oxygen or water. Interestingly, while the CO_2 to CO intensity ratio is close to unity for the Ar and O_2 plasma, the CO signal is now much stronger than the CO_2 signal. Finally, C_2F_5 has been detected at an amu/q of 119 (not shown), indicating the recombination of fluorocarbon fragments into larger molecules.

Once all the gases are combined, behavior belonging to simple oxygen and CF_4 plasmas are merged. There is a production of CO and CO_2, as well as COF and COF_2, accompanied by an important consumption of CF_3 and O_2. For the first time, CF_2 is consumed as well. Fluorine is still missing from the spectra, while C_2F_5 is not detected anymore.

The observations made from Figure 4.1 match those of the literature. They first indicate that CF_4 dissociates into CF_x fragments. Amongst those fragments, CF_3 and CF_2 are oxidized to form CO, CO_2, COF, and COF_2. However, little fluorine is detected from the plasma. Since CF_4 dissociation was confirmed, and since such dissociation necessarily implies the formation of F, we conclude that the absence of F peak in the spectra is due to its inability to reach the spectrometer's detector, and not from a total absence of F in the reactor. In a similar manner, the important losses of CF_3 occurring when the plasma is ignited suggest important CF_3 dissociation and oxidation. Considering that those CF_3-consuming reactions produce

atomic fluorine, the absence of atomic F from the spectra again suggests that no F reaches the spectrometer.

We explain the absence of F by fast recombination with sputtered Al. Indeed, by providing a continuous flux of recombination partners, Al and F would easily react before F is detected. As no aluminum fluorides (AlF_3 - 84 amu/q, AlF_2 – 65 amu/q, AlF – 46 amu/q) were detected in the mass spectra, the fluorine recombination is assumed to take place on surfaces, effectively depleting the gas phase. Since CF_3 can also recombine through third bodies, part of its observed intensity reduction is attributed to recombination, in addition to consumption by reactions.

When only using CF_4 as a reactive gas (Figure 4.1 c), CF_2 production by fragmentation of larger fluorocarbons dominates over CF_2 consumption by oxygen, leading to a positive peak at 50 amu/q. However, when adding O_2 to the CF_4, the consumption by oxygen dominates, and the CF_2 signal becomes negative. This underlines the importance of reaction **??** for the enrichment of atomic fluorine via the addition of oxygen. Finally, the disappearance of C_2F_5 indicates that the polymerization reactions observed in the CF_4 plasma are blocked by the addition of oxygen. The oxidation of CF_3 and CF_2 indeed makes those species unavailable for agglomeration in large molecules.

Effect of power and oxygen flow on the plasma composition

To better understand the effect of sputtering on species concentration and recombination, spectra of an $Ar/O_2/CF_4$ sputtering discharge were acquired at different sputtering powers and different oxygen flows. A good characterization of the fluorine concentration's responses to those parameters is important in order to deposit coatings with maximal fluorine content. The effect of power at constant input of oxygen is presented first in Figure 4.2, which shows the relative variation in the intensity of the major species found in the plasma as a function of power. To illustrate their relative variation, the recorded peak intensity of each species was normalized by the species' intensity at 50 W. Apart from power, all other experimental parameters were kept constant (pressure of 2 mTorr, gas flow of 15 sccm for Ar, 5 sccm for O_2, and 5 sccm for CF_4).

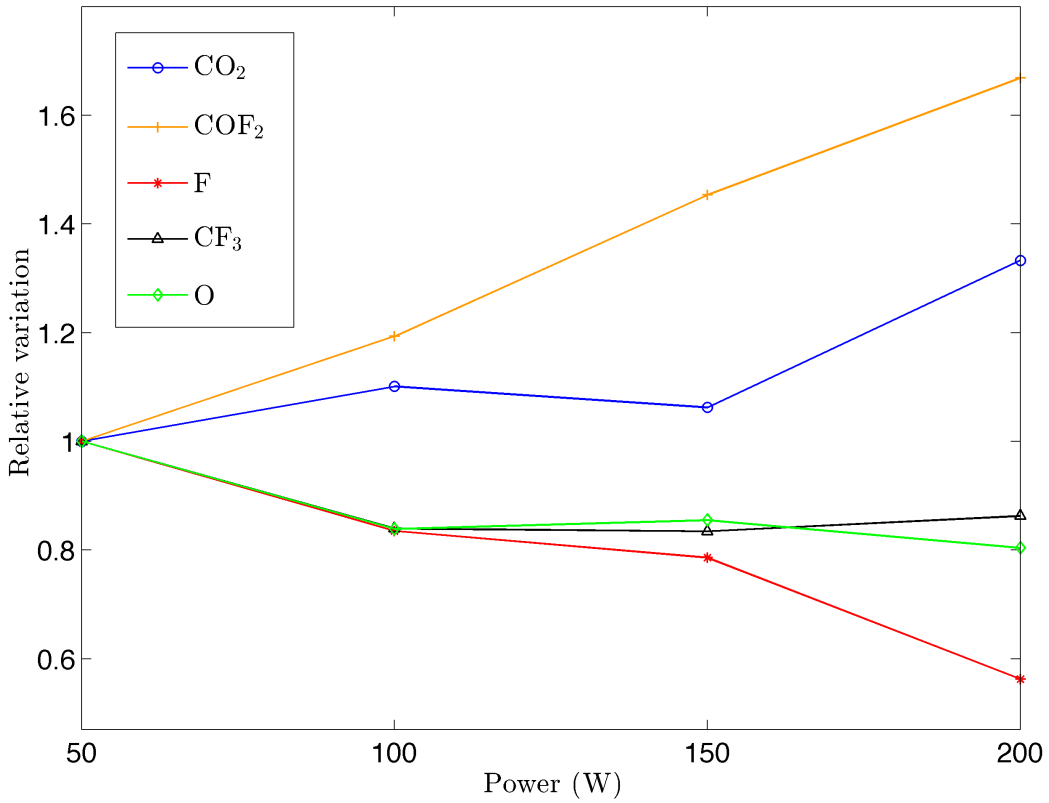

Figure 4.2 Intensity variation as a function of magnetron power for the main species found in the plasma. Variation normalized to unity at 50 W. Plasma containing Ar (15 sccm), CF_4 (5 sccm) and O_2 (5 sccm) at 20 mTorr.

It was established in Section 4.2.1 that in an $Ar/O_2/CF_4$ sputtering discharge, CF_4, CF_3, CF_2, and O_2 were initial reactants while F, CO_2, COF_2, and their fragments were reaction products. It was also shown that the plasma gas phase was poor in F due to recombination with sputtered species. Figure 4.2 demonstrates that elevated powers intensify those reactions. The increase in power is followed by an increase in COF_2 and CO_2, and by a decrease in atomic O, CF_3, and atomic F. The other CF_4 fragments (not shown) also follow a downward trend. The molecular oxygen (not shown) stays constant, suggesting that the flux of injected O_2 balances out the losses due to reactions.

CF_3 and O intensities both decrease between 50 and 100 W. Such a covariance suggests that they react together through Reaction **??** to produce atomic F and COF_2. Since the intensity loss plateaus after 100 W but the production of COF_2 does not, we expect other reactions to take over at high powers and form COF_2.

The atomic fluorine intensity decreases rather linearly with power, which supports the re-

combination through sputtered Al hypothesis. Indeed, higher sputtering powers increase the sputtering rate of the Al target, although the relationship is not always linear during reactive sputtering. It remains to determine if the AlOF coatings get richer or poorer in fluorine as third-body recombination becomes more important.

We have so far assumed that the sputtered species participating in recombination were metallic aluminum. However, in a reactive plasma, the density and nature of the sputtered species depend on target surface condition. In the present case, severe poisoning of the target is observed, as shown in Figure 4.3. In pure CF_4 discharge (0 sccm of O_2), the target is already poisoned by fluorocarbon. The subsequent addition of oxygen aggravates the poisoning by oxidizing the target. Hence, the sputtered material transitions from C-F-Al compounds in low-O_2 gas mixtures, to oxides in O_2-rich mixtures, where the sputtering yield is poor. This reduction in sputtering rate is surely decreasing the number of sputtered recombination partners for fluorine and could contribute somewhat to the increase in F concentration as a function of O_2 flow.

In addition to sputtering power, the concentration of oxygen in the gas feed also has an important effect on the plasma chemistry and has the potential to impact greatly the composition of the AlOF coatings. Figure 4.4 presents the relative variation of mass peak intensity for the main species of the plasma.

Figure 4.4 shows that oxygen increases the concentration of fluorine in the sputtering plasma, as observed by the plasma etching community [13,53,57,58]. However, the relative increase is small, less than 1.5 times the initial intensity, which is much less than the tenfold increase in F observed in other studies [13]. The CF_3 concentrations decrease as a function of O_2 intake, which again corroborates that it reacts with oxygen to form COF_2 and CO_2. Figure 4.4 also demonstrates that oxygen-containing species increase in concentration when oxygen is initially added to the gas mixture, but that this relationship is not linear. For CO_2, the signal increases by a factor of 20 when 10 sccm of O_2 is added to the gas mixture. COF_2 and COF co-vary while CO varies in an opposite fashion. This opposite trend between CO and carbonyl fluorides suggests that CO is involved in their production, through reactions with atomic and molecular fluorine.

As for the effect of power, it remains to establish the relationship between oxygen flow and AlOF composition. Specifically, fluorine concentrations and carbon contamination can both be potentially impacted by the quantity of oxygen employed.

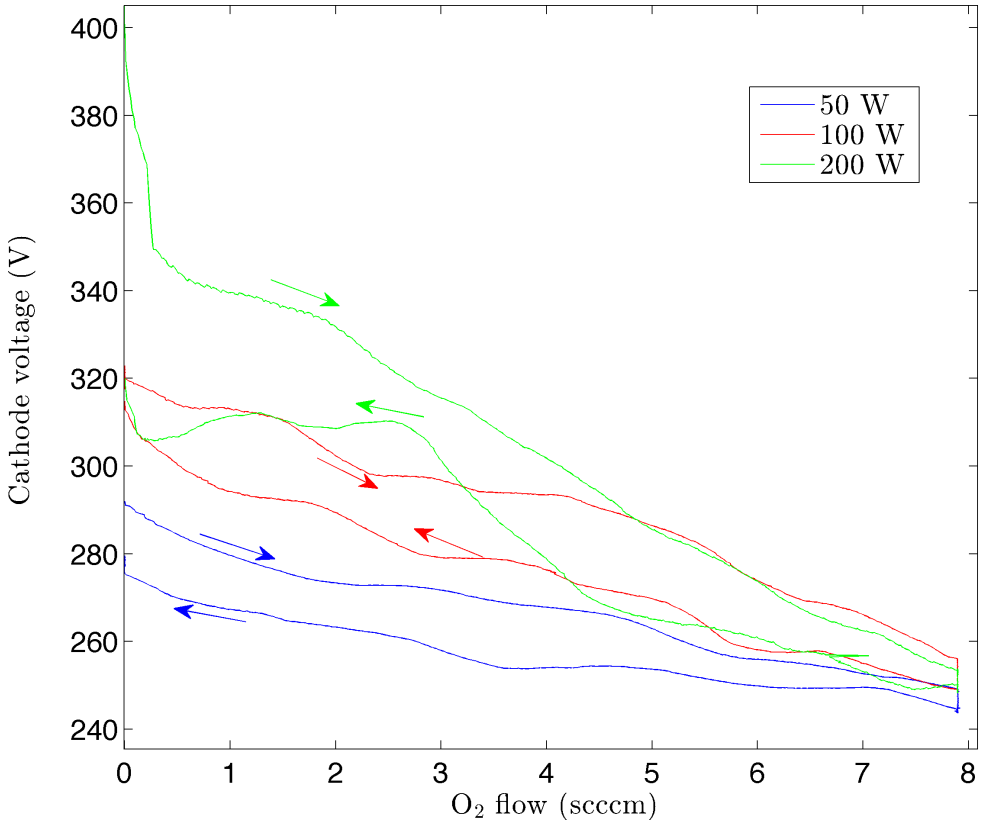

Figure 4.3 Cathode voltage hysteresis of a sputtering $Ar/O_2/CF_4$ discharge as a function of oxygen flow at different sputtering power. Pressure was held constant at 20 mTorr, CF_4 flow was kept constant at 5 sccm.

4.2.2 Coating composition

An interesting dynamic has been established in Section 4.2.1, where high sputtering powers decrease the concentration of fluorine by favoring recombination, while high oxygen contents increase atomic F. The relationship between gas phase and chemistry of the deposited AlOF coatings now needs to be established in order to deposit films with optimized chemical composition. AlOF coatings were therefore deposited on TiAl using different sputtering powers and oxygen flows, as summarized in Table 4.1. As with the gas phase composition study, the power was first varied from 50 W to 200 W while keeping the oxygen flow constant at 5 sccm. Then, while maintaining a constant power of 200 W, the oxygen flow was varied from 0.5 to 5 sccm. These combinations of power and O_2 flow were chosen to mimic the mass spectrometry study of Section 4.2.1.

The other deposition parameters were kept constant for all depositions. The CF_4 flow was

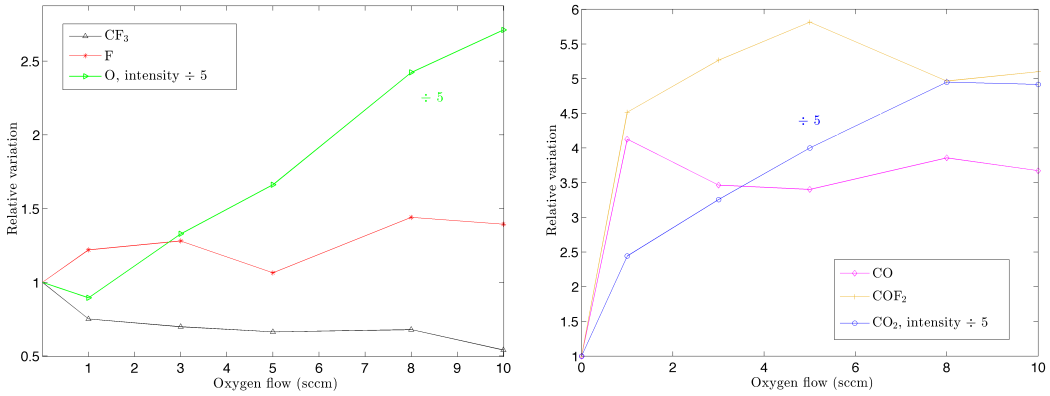

Figure 4.4 Relative variation of the main species' intensity as a function of oxygen flow in the plasma reactor, split in two groups for visual clarity; Values are normalized to unity at 0 sccm of O_2. Plasma powered by 150 W, containing Ar (15 sccm), CF_4 (5 sccm) and O_2 at 20 mTorr. CO_2 and O_2 signals are downscaled for easier visual comparison.

8 sccm, to ensure maximal fluorine concentration in the AlOF coatings and optimal performance of the halogen effect. The pressure was kept at 20 mTorr, and Ar flow was kept at 15 sccm.

Table 4.1 Choice of sputtering power and oxygen flow for the study of AlOF composition. Other deposition parameters are kept constant (pressure of 20 mTorr, Ar flow of 15 sccm, CF_4 flow of 8 sccm).

Sample ID	A-50-5	A-100-5	A-150-5	A-200-5	A-200-3	A-200-1.5	A-200-0.5
Power on target (W)	50	100	150	200	200	200	200
O_2 flow (sccm)	5	5	5	5	3	1.5	0.5

RBS measurements confirm the coating composition of Al26-O6-F60-C5 on average, with common contaminants being Cr and of V at concentrations smaller than 1 at.%. The coating composition is almost independent of oxygen flow and discharge power, as seen in Figure 4.5. The coatings' composition is close to that of AlF_3 doped with O and C.

Figure 4.5 a) shows the variation of the coatings compositions as a function of power. Fluorine content marginally increases with power. This is consistent with the fact that fluorine gains access to more recombination partners at increased powers and sputtering rates. The deposited species are enriched in F by reactions at the surface of TiAl. At the same time, aluminum decreases as a function of power. Oxygen stays constant while carbon slightly increases.

In Figure 4.5 b), the fluorine concentration in the coatings does not really increase with the

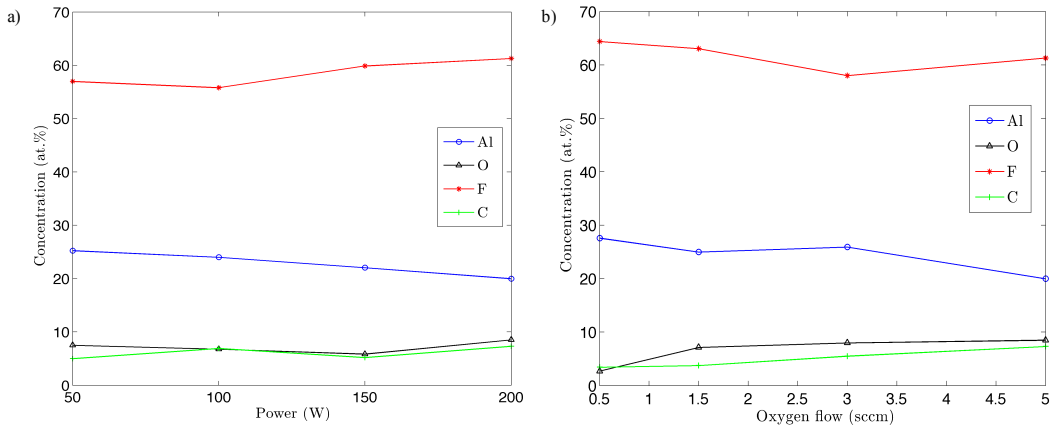

Figure 4.5 Evolution of coatings' composition as a function of a) power (at a constant 5 sccm O_2 flow) and of b) oxygen flow (at a constant power of 200 W). Other plasma parameters are kept constant, with a pressure of 20 mTorr, Ar flow of 15 sccm, CF_4 flow of 8 sccm.

addition of oxygen. Oxygen concentrations increase with the oxygen flow, as do carbon. Aluminum compensates for these increases. It was previously established that oxygen-rich plasmas increased the concentrations of F in the gas phase. It seems that this enrichment in F does not translate into F-rich coatings. The carbon increase with O_2 flow is rather surprising, as it was expected that the important production of volatile CO and CO_2 at high oxygen flows would evacuate a lot of carbon from the reactor. Perhaps that the carbon contamination is due to carbon dioxide trapping due to the extreme CO_2 quantities produced in the gas phase at high oxygen content (see Figure 4.4 a).

The coating containing the most fluorine was produced at 200 W and 0.5 sccm of O_2. However, their composition does not differ a lot from the other AlOF coatings.

4.2.3 Oxidation performance of selected coatings

Although no strong link can be established between the sputtering parameters and the chemical composition of the coatings, other properties of the coatings like their microstructure or adherence to the substrate can be influenced by the choice of power and oxygen flow. To account for those effects and see if power and oxygen flow have an effect on the oxidation behavior of AlOF, coatings were produced using three combinations of parameters. Coatings were deposited at high power and low oxygen flow (200 W, 0.5 sccm O_2), high power and high oxygen flow (200 W, 5 sccm O_2), and low power and high oxygen flow (100 W, 5 sccm O_2).

The AlOF coatings were deposited on γ-TiAl, along with a 200 nm-thick aluminum interlayer.

The Al layer acts as a bond coat and potentially mitigates Al depletion in TiAl, a recurring phenomenon due to the formation of Al_2O_3 leading to excessive Al pumping out of the TiAl after high-temperature oxidation [10]. To ensure reproducibility, the depositions have been repeated two times. The specific deposition conditions are listed in Table 4.2. The AlOF and interlayer thicknesses were measured on SEM cross-sections micrographs and corroborated by mechanical profilometry measurement of the total thickness. The thickness of two of the coatings couldn't be accurately measured with SEM due to important damage during the preparation of the cross-section. Their combined thickness according to profilometry measurements is of 0.68 μm for sample B-200-0.5-ii, and of 0.41 μm for sample B-200-5-i.

Table 4.2 Deposition conditions for the oxidation test. Three different coating types were tested, with two samples produced for each type. Some deposition parameters were common to all samples, namely the pressure (20 mTorr), the Ar flow (15 sccm), and the CF_4 flow (8 sccm).

Sample ID	Power (W)	Oxygen flow (sccm)	AlOF thickness (μm)	Al interlayer thickness (μm)
B-200-0.5-i	200	0.5	0.43	0.18
B-200-0.5-ii	200	0.5	n.a.	n.a.
B-200-5-i	200	5	n.a.	n.a.
B-200-5-ii	200	5	0.54	0.21
B-100-5-i	100	5	0.57	0.24
B-100-5-ii	100	5	0.46	0.15

The chemical composition of the AlOF layer before oxidation is measured by RBS and is again independent of deposition conditions, averaging at an atomic composition of Al26-O14-F59-Cr1, with no more C and V contamination being detected. SEM micrographs of the coatings' surfaces are shown in Figure 4.6, while a typical coating cross-section micrograph with corresponding EDS chemical maps is shown in Figure 4.7.

Sample surfaces present some defects in the forms of spheres and craters, with samples B-200-0.50-i and ii being the most affected. The defects have a diameter in the range of the micrometer. EDS mappings show that their chemical composition is that of the surrounding AlOF, rather than that of exterior contaminants like dust or oxide. The sputtering process is therefore prone to the production of large particles. The exact origin of those particles is unknown. Dust formation, which is known to occur in fluorocarbon plasmas could be responsible, as could be sputtered droplets caused by arcing between the magnetron and the Al target, a common phenomenon in reactive sputtering discharges [59].

The cross section micrograph shows a uniform 0.5 μmm thick coating which was identified as

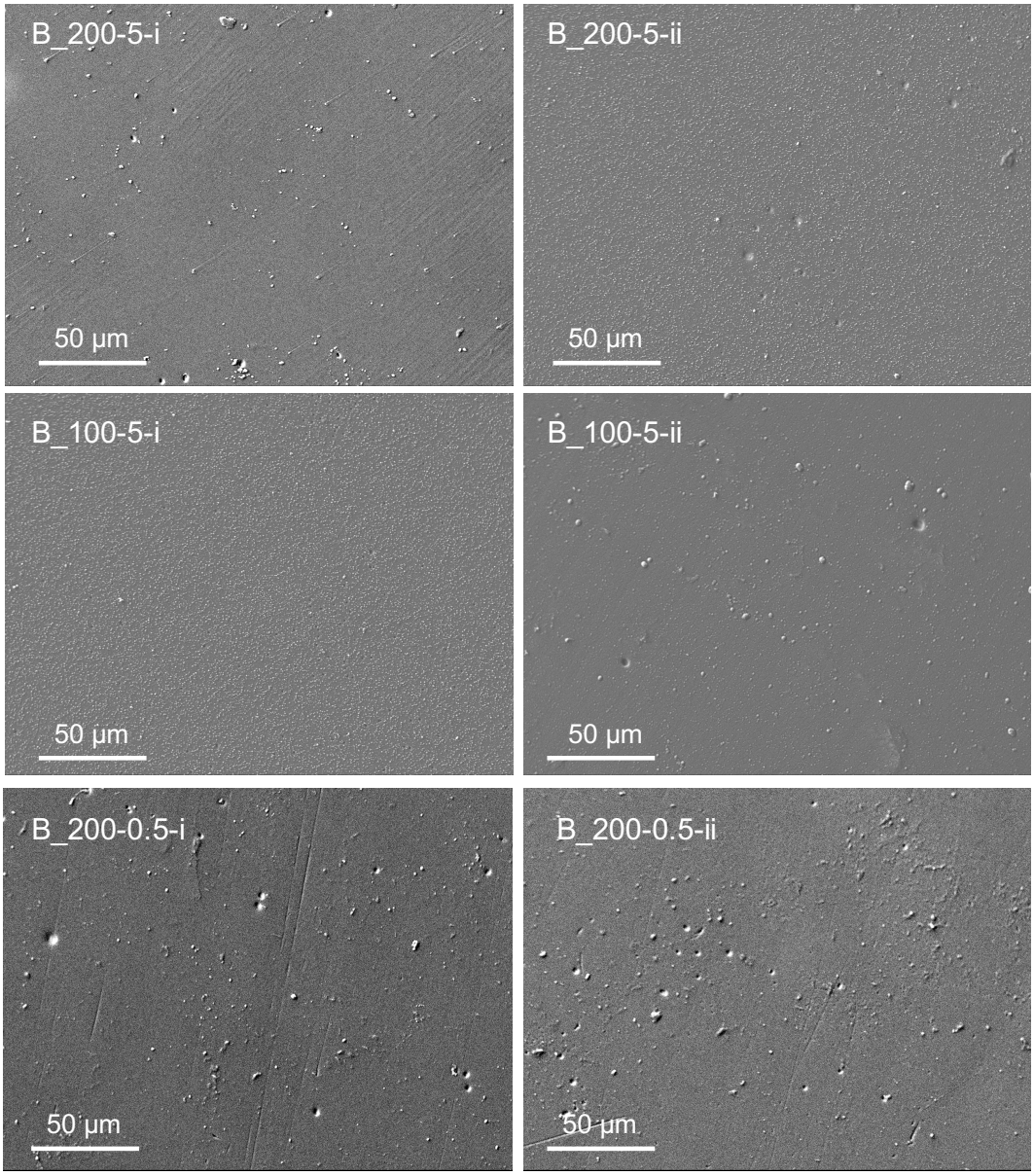

Figure 4.6 SEM surface micrographs of coatings prepared for oxidation.

being AlOF by complementary EDS and RBS measurements. The thin 200 nm Al interlayer is also visible. According to the RBS measurements, the AlOF layer is uniform, i.e. no composition gradient or other internal structure is identified.

Oxidation tests

Oxidation tests were performed at 875 °C in laboratory air, followed by manually weighing the samples. Mass gains as a function of oxidation time are presented in Figure 4.8. A bare TiAl

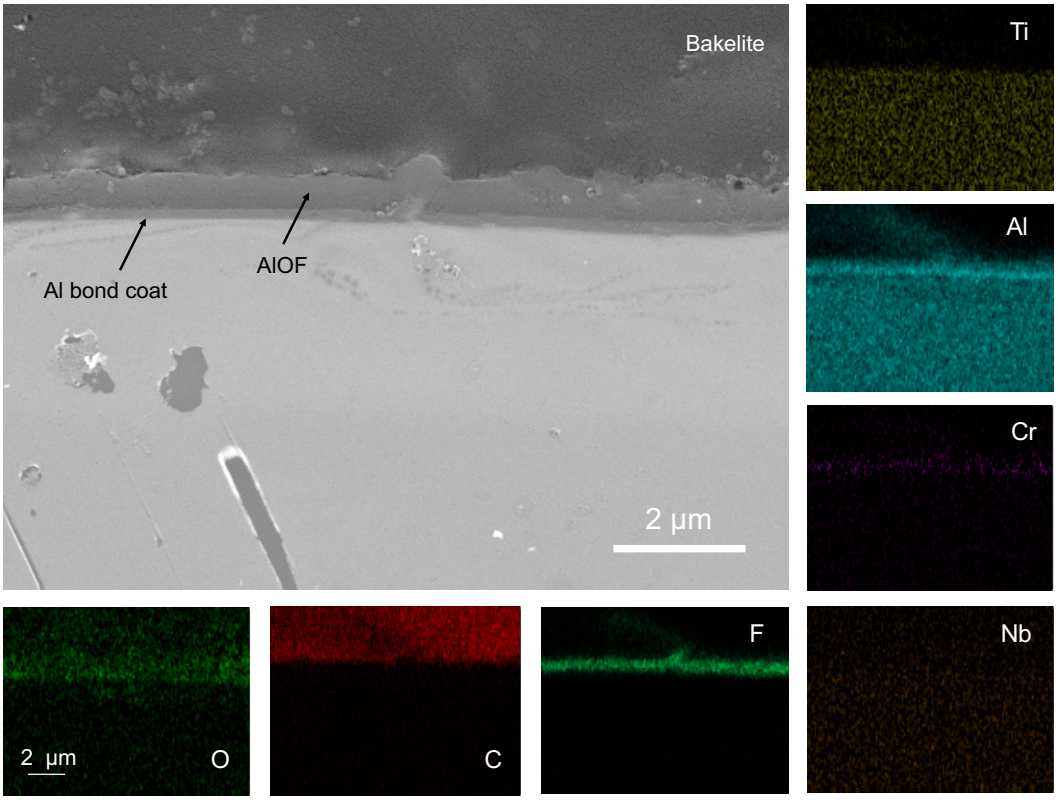

Figure 4.7 SEM micrograph of sample B-200-5-ii's cross-section before oxidation along with EDS chemical maps. The sample was mounted in bakelite, which is visible in the top quarter of the micrograph.

substrate was also oxidized for comparison purposes. Rapid mass gains were observed for the bare TiAl, followed by important oxide spallation after 25 hoursmof oxidation, resulting in an important mass loss. The coated samples showed smaller mass gains.

The fluorine-rich coatings prepared at high power (200 W) and low oxygen flow (0.5 sccm) offered the best initial protection but suffered important mass gains after 25 h. The best long-term protection was offered by coatings produced with 5 sccm of oxygen, by either using 100 W or 200 W of RF power. Mass gains are low, and the thin oxide scale produced is composed of aluminum oxide. The oxide thicknesses measured on SEM cross-section micrographs after oxidation on the four samples with the lowest mass gains ranged from 1.5 to 2.8 μm depending on the location across the samples. Figure 4.9 shows such a cross section and the corresponding EDS chemical map. The oxide scale, visible on the oxygen and aluminum maps, was about 2.5 μm thick and contained very little titanium. In some locations, like on the left of the micrograph, a mixed titanium and aluminum oxide was present on top of the continuous layer of alumina. This is due to the growth of titanium

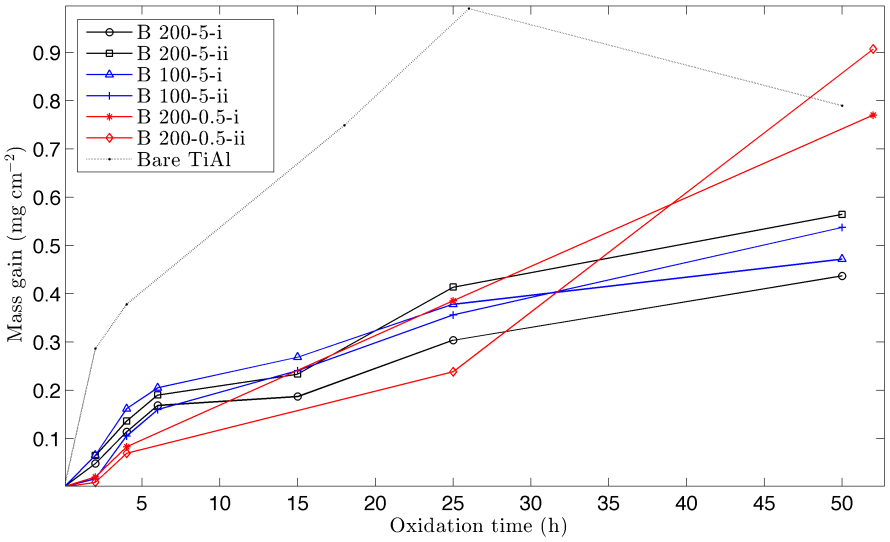

Figure 4.8 Mass gain of different AlOF coated samples at 875 °C. A bare TiAl substrate is shown for comparison.

oxide in the initial stages of oxidation [60]. Some fluorine remained in the oxide scale after 50 h of oxidation, which indicates that the halogen effect can sustain itself for longer periods of time.

Rapid variation in the oxidation pattern, like the one observed for the 200 W and 0.5 sccm coatings, suggests that some coating failure occurred, upon which the substrate became more vulnerable to oxygen. SEM micrographs of the coatings surface, as seen in Figure 4.6, show that B-200-0.5i and B-200-0.5ii bore numerous defects in comparison to the other coatings. The presence of defects implies poor local oxidation protection and eventual crack initiation at the defects, particularly if the coating is submitted to thermal and oxide-growth related stresses.

As the oxidation performances of samples produced at 200 W and 100 W and 5 sccm of O_2 were similar, but the deposition rates were three times higher when using 200 W, the 200 W and 5 sccm coatings were chosen at the most interesting. The optimized deposition conditions for the AlOF coating are 200 W applied on Al target, 20 mTorr, 5 sccm O_2, 15 sccm Ar,

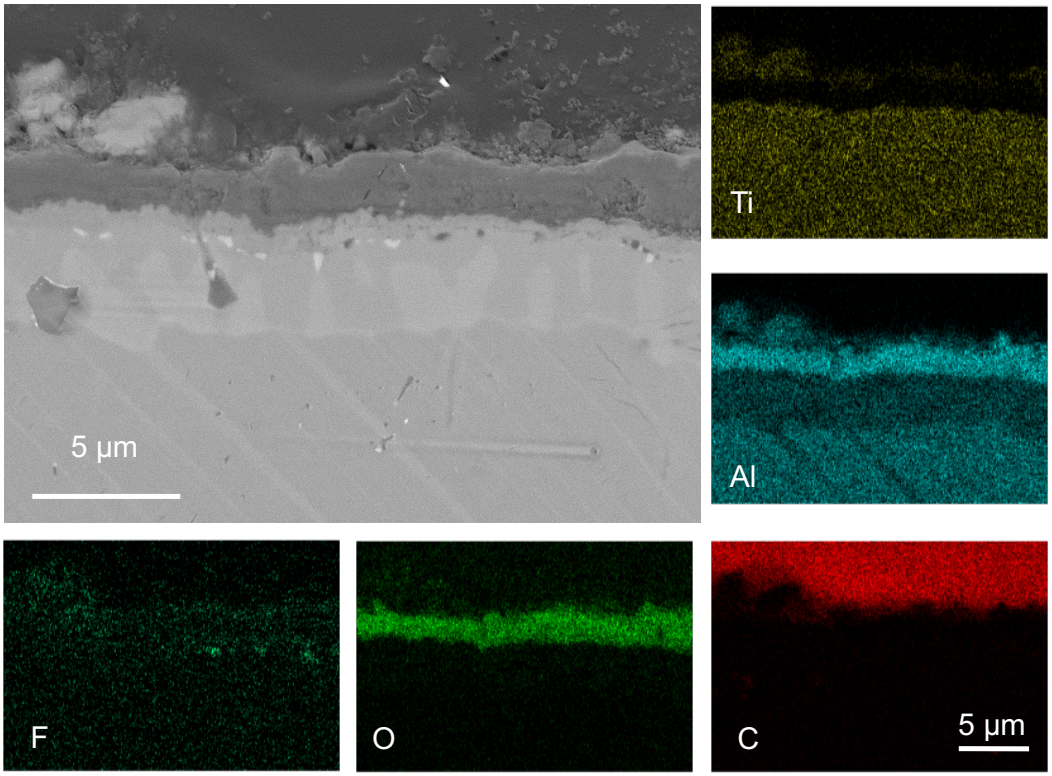

Figure 4.9 SEM cross section and the corresponding EDS chemical maps for sample B-200-5-i after oxidation at 875 °C for 50 hours.

8 sccm CF_4.

4.2.4 Impact of AlOF thickness on oxidation protection

The amount of fluorine provided to the AlOF is primordial to the good performance of the halogen effect. Indeed, a low fluorine flow will not produce enough aluminum fluoride to sustain alumina formation. On the other hand, too much fluorine will promote the formation of titanium fluorides, which will compete with aluminum fluorides to form the oxide. Since the sputtering parameters have little effect on the fluorine content of the AlOF coatings, thickness variation is the only way to provide the TiAl with more or less of this halogen. To optimize the thickness of the AlOF coatings, thin (0.5 μm), medium (1.3 μm) and thick (2.3 μm) AlOF coatings were deposited on TiAl with a 200 nm Al interlayer. The optimized deposition conditions from Section 4.2.3 were used (200 W of sputtering power, 5 sccm of O_2 flow, 15 sccm of Ar, 8 sccm of CF_4, 20 mTorr). The mass gains of the different samples are presented in Figure 4.10.

Thin coatings showed the highest mass gains after, which indicates that the total intake

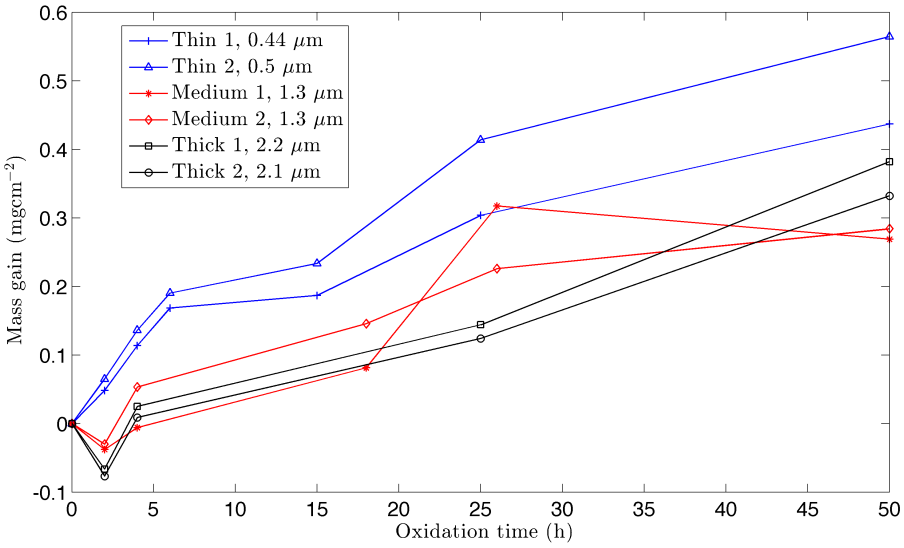

Figure 4.10 Effect of AlOF coating thickness on mass gains during isothermal oxidation at 875 °C for 50 h.

of fluorine was not sufficient to reach the halogen effect's full potential. Initially, the thick coatings showed small mass gains but steadily oxidize in a rather linear fashion. They overtake the AlOF of medium thickness after 40 hours of oxidation. It is difficult to truly distinguish between the medium and thick coatings after only 50 hours of oxidation. However, it is clear that one would benefit from coatings that are more than 0.5 μm thick.

4.2.5 Oxidation kinetics of Al/AlOF coatings

The same optimized coating was then redeposited several times and oxidized at different temperatures, namely, 750 °C, 775 °C, 800 °C, 850 °C, and 875 °C. The mass gain curves as a function of time at those temperatures allowed the calculation of the oxidation rate constant k_n in mg^n cm^{-2n} h^{-1}, by fitting the curves with Eq. 2.1. Figure 4.11 shows the mass gain for the different oxidation temperatures and Table 4.3 lists the fitted reaction rates and corresponding exponents.

Reaction rates increase with the oxidation temperature, reaching 7 mg cm^2 at 875 °C. This

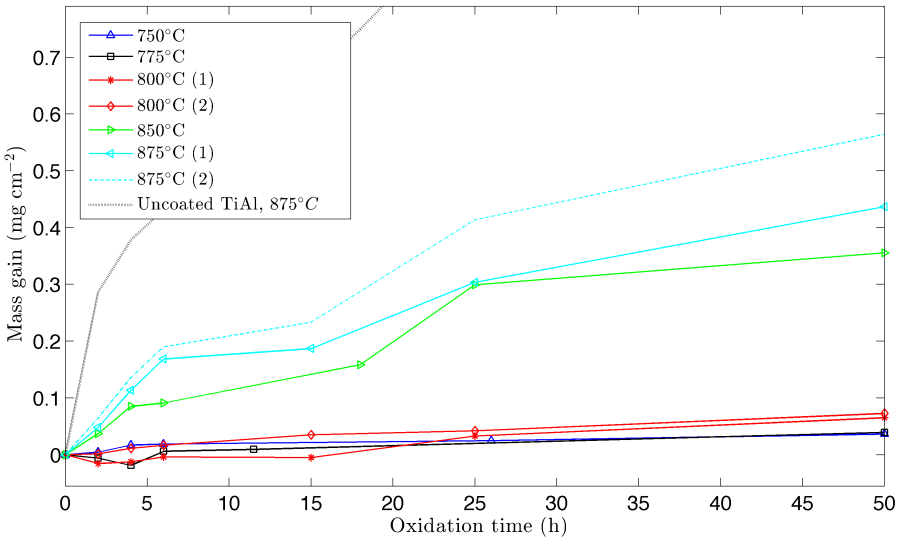

Figure 4.11 Mass gain of coating B-200-5 during oxidation at different temperatures

value is well below the of unprotected Ti-48Al-2Nb-2Cr, which is of 20 mg cm^2 at that same temperature. Literature reports k_n of 49.7 7 mg cm^2 and 120.0 7 mg cm^2 for oxidation at 850 °C and 900 °C respectively [61]. Fluorine implantation has been shown to reduce the oxidation reaction rates to between 0.44 and 1.1 mg cm^2 at 900 °C [62, 63]. Other overlay metal-CrAlY coatings have shown parabolic rates between 3.5 mg cm^2 and 19.9 mg cm^2 [64,65]. The AlOF-coated TiAl have higher oxidation rates than those that were F-implanted, but show similar kinetics as those of other overlay coatings. The overlay coatings are more susceptible to defects, loss of adhesion and other coating failures. This may explain their faster oxidation when compared to halogen-implanted TiAl.

When oxidized at low temperatures (750 °C to 800 °C), some samples experienced weight losses. Those losses are usually attributed to evaporation of carbon compounds in the coatings [37]. Those coatings were difficult to fit with Eq. **??**, as their curves did not initially follow a parabolic trend. Those coatings have oxidation exponents close to unity in Table 4.3 and were not considered in the rest of the computations.

Using parabolic rates only and their associated oxidation temperatures, the activation energy

Table 4.3 Oxidation reaction rates k_n and exponents n for different oxidation temperatures.

Oxidation temperature (°C)	k_n [mg^n cm^{-2n}h^{-1}]	n
750 (sample 1)	0.00	3
775 (sample 1)	0.6	1.1
800 (sample 1)	1.2	1.02
800 (sample 2)	0.5	1.4
850 (sample 1)	4	1.6
875 (sample 1)	4	1.8
875 (sample 2)	7	1.8

Q in kJ mol^{-1} of the Al+AlOF coating was calculated. The parabolic oxidation rate k_p is related to the activation energy according to Eq. 2.2. Transforming this equation to facilitate linear regression gives

$$\ln k_p = \ln k_0 - \frac{Q}{RT} \tag{4.1}$$

The resulting regression yields an activation energy of 312± kJ mol^{-1}. Previous studies found activation energies for unprotected Ti-48Al-2Nb-2Cr between 138 and 216 kJ mol^{-1} [61, 66]. The high calculated activation energy and reaction rates lower than those of bare TiAl indicate that the AlOF coating offers oxidation protection and slows the oxidation of the TiAl.

4.3 Conclusion

Aluminum-oxy-fluoride coatings deposited by reactive RF magnetron sputtering were shown to efficiently protect TiAl against high-temperature oxidation up to 875 °C. The plasma chemistry, investigated by mass spectrometry, revealed that high RF powers reduced the concentration of atomic fluorine in the coating due to increased fluorine recombination with sputtered species. This leads to deposited coatings that are somewhat richer in fluorine when high sputtering powers are used. However, the sputtering parameters have weak impacts on the composition of the AlOF, and the observed variations in chemical content are small.

Plasma chemistry also revealed that the fluorine concentrations followed the amount of molecular oxygen injected in the plasma. This increase in fluorine in the gas phase due to oxygen does not impact the concentration of fluorine deposited on the TiAl. This indicates that a gas phase that is fluorine-rich is not sufficient for the deposition of fluorine-rich coatings. High fluorine reactivity with surfaces provided by high sputtering powers has the most impact on

coating composition.

Seemingly because of a high concentration of defects, coatings produced with small oxygen flows do not perform well in oxidation tests. The best-performing coatings were those deposited at high flows (5 sccm). The coatings were comprised of Al26-O6-F60-C5 and showed mass gains significantly lower than those of uncoated samples after 50h of oxidation at 875 °C. The oxidation kinetics are slowed by an order of magnitude, and the activation energy for oxidation was increased by the presence of AlOF. The formed oxide scales are mostly made of aluminum oxide with some residual F present, maintaining long-term protection through the halogen effect.

CHAPTER 5 DISCUSSION

The results presented in Section 4 show that sputtered AlOF films can protect TiAl against high-temperature oxidation. The mass gains at the highest oxidation temperature (875 °C) were between 0.44 and 0.56 mg cm^{-2} after the 50 h isothermal test. For the same oxidation time, but for tests performed at 900 °C, the literature shows mass gains 0.23 and 1.52 mg cm^{-2}, with most of the values falling above 0.6 mg cm^{-2}. Table 5.1 summarizes those values. The mass gains listed were read out of thermogravimetric analysis (TGA) curves presented in articles, and not quoted by the authors themselves. Hence, they are somewhat approximate. If an article presented many variants on one type of coating, only the best recipe was tabulated.

Table 5.1 Mass gains of different TiAl samples protected by the halogen effect according to literature. The isothermal oxidation tests were performed at 900 °C in laboratory air. PI^3 refers to plasma immersion ion implantation, where the halogens ions in a plasma are accelerated toward and implanted in a heavily-biased sample (biases in the kV range). BI^2 refers to beamline ion implantation, where an ion accelerator is used to implant the halogen. The CF_x vapor technique implies the exposure of a TiAl sample for 15 minutes to mixture of fluorocarbon and oxygen heated at 900 °C. The heat and oxygen oxidize the TiAl, while the fluorocarbon activates the halogen effect The diluted HF technique uses a 0.1 wt.% HF dilution in water. The samples are dipped in the solution for many hours.

Halogen	Method	Mass gain after 50 h (mg cm^{-2})	Reference
F	PI^3	0.61	[38]
F	PI^3	1.06	[67]
F	PI^3	0.62	[68]
F	PI^3	0.23	[62]
F	BLI^2	0.56	[38]
F	BLI^2	1.32	[67]
F	Diluted HF	0.34	[62]
F	CF_x vapor	0.25	[62]
F	Diluted HF	0.37	[69]
Cl	BLI^2	1.36	[3]
Cl	BLI^2	1.52	[33]
Cl	BLI^2	1.47	[70]
Br	BLI^2	1.11	[33]
I	BLI^2	1.29	[33]

The experiments presented in Table 5.1 were performed at temperatures 25 °C superior to this thesis's tests. However, the mass gains of the AlOF coatings is comfortably below that

of other techniques like BLI[2] and PI[3], which are considered to be well working. It is not too far fetched to assume that AlOF coatings would also perform well at 900 °C.

However, the articles cited in Table 5.1 tested the protectiveness of their coatings for periods longer than 50 h, which we couldn't do due to time constraints. There is no information on the long-term performances of those new coatings, and it is primordial to investigate this aspect further to guarantee that the solution can be implemented in industry.

The oxidation rates of the AlOF coatings, obtained by fitting the mass gains of Figure4.11 at 875 °C with Eq. 2.1 can also be compared against those of literature for halogen effect. Not all studies calculate this rate, but Table 5.2 presents those which did. Again, if more than one coatings were deposited, only the most protective is shown in the table.

Table 5.2 Oxidation rates of different TiAl samples protected by the halogen effect according to literature. The isothermal oxidation tests were performed at 900 °C in laboratory air.

Halogen	Method	Parabolic rate at 900 °C ($\times 10^{-3} mg^2 cm^{-4} h^{-1}$)	Reference
F	PI[3]	1.0	[62]
F	BLI[2]	1.1	[62]
F	BLI[2]	0.44	[63]
F	Gas phase	1.3	[62]
F	HF dipping	2.6	[62]
P	BLI[2]	22.0	[71]

The AlOF parabolic oxidation rate is of $7.0 \times 10^{-3} mg^2 cm^{-4} h^{-1}$, which is superior of those listed in the literature. More work is required to match the low oxidation rates of the F-implanted samples. It is however believed that AlOF is a promising solution, although it remains to be optimized.

Another drawback of the methodology was that the isothermal oxidation tests were not performed in a TGA system. This would have allowed the samples to be weighed in real time during oxidation, without removing them from the oven. Instead, they had to be taken out and cooled frequently. This is most detrimental to the early mass gain measurements, where the "isothermal" tests were not really isothermal anymore. Cyclic oxidation could perhaps better describe this section of the tests. Cyclic and isothermal oxidation are not modeled using the same parameterization. Therefore, when fitting the mass gain curves, it is not strictly correct to fit the early oxidation with a parabolic oxidation curve. It was done in this fashion for the sake of simplicity. The agreement between the fitted curves and the experimental data was therefore bad in the early stages of oxidation, particularly at the low oxidation temperatures shown in Figure 4.11.

The cyclic oxidation resistance should also be investigated. It is known that fluorine offers good protection in such environments, but overlay coatings are known to be susceptible to failure when undergoing repetitive changes in temperatures. However, the severe air quenches and rapid re-heating during the weighing sessions are indicators that the coatings should perform well.

CHAPTER 6 CONCLUSION

The results presented in the thesis show that sputtered AlOF coatings offer effective protection against high-temperature oxidation of TiAl 48-2-2. Protection up to 875 °C has been demonstrated during isothermal oxidation tests in laboratory air. The oxidation rates were smaller than those of unprotected TiAl. The oxidation activation energy of the AlOF was calculated to be 312 ± 141 kJ mol^{-1}, which is higher than for unprotected TiAl. This demonstrates that the AlOF coatings slow down the oxidation of the substrate.

The reactive sputtering process leading to the coatings has been diagnosed using mass spectrometry. Using plasma etching gas phase chemistry as a base, the behavior of the sputtering plasma could be understood as power and oxygen flow were varied. The reduction of atomic fluorine and of CF_3 signal intensities as the sputtering power is increased was attributed to an increase in the number of metallic recombination partners. The addition of oxygen to the plasma increased the concentration of fluorine in the gas phase, a phenomenon that is well documented. The variations of the gas phase composition as a function of power and oxygen flow had little impact on the composition of the AlOF coatings, which were roughly composed of Al(26)-O(6)-F(60)-C(5). Elevated powers and larger oxygen concentrations in the plasma produced the coatings offering the best oxidation protection.

The AlOF coatings have not been tested at temperatures higher than 875 °C, and were oxidized for short periods of times. To be truly certain of their protective potential, it is primordial to conduct longer tests at higher temperatures. The cyclic oxidation resistance should also be investigated. The coatings have also not been tested on complex-shaped surfaces. Sputtering is a rather line-of-sight process. Although the samples are rotated during deposition, conformality is not guaranteed on particularly complex shape, which can complicate the implementation of this coating in the industry.

Future research on the AlOF coatings should also include mechanical properties test on the coatings themselves, but also on the coating and substrate system as a whole. Indeed, it is important to know what kind of wear and erosion resistance the coating can offer, and it is primordial to ensure that the fluorination of the TiAl does not modify its basic mechanical properties. In particular, no embrittlement should follow the application of the coating. Simple tensile tests on coated and uncoated specimens would provide valuable insight into this potential problem.

BIBLIOGRAPHY

[1] Y. Mishin and C. Herzig, "Diffusion in the Ti-Al system," *Acta materialia*, vol. 48, no. 3, pp. 589–623, 2000.

[2] R. Kainuma, M. Palm, and G. Inden, "Solid-phase equilibria in the Ti-rich part of the Ti-Al system," *Intermetallics*, vol. 2, no. 4, pp. 321–332, 1994.

[3] A. Donchev, B. Gleeson, and M. Schütze, "Thermodynamic considerations of the beneficial effect of halogens on the oxidation resistance of TiAl-based alloys," *Intermetallics*, vol. 11, no. 5, pp. 387–398, 2003.

[4] D. Depla, S. Mahieu, and J. Greene, "Chapter 5 - Sputter Deposition Processes," in *Handbook of Deposition Technologies for Films and Coatings (Third Edition)*, third edition ed., P. M. Martin, Ed. Boston: William Andrew Publishing, 2010, pp. 253 – 296. [Online]. Available: http://www.sciencedirect.com/science/article/pii/B9780815520313000053

[5] "IATA forecast predicts 8.2 billion air travelers in 2037," *The International Air Transport Association*, Oct 2018. [Online]. Available: https://www.iata.org/pressroom/pr/Pages/2018-10-24-02.aspx

[6] B. Bewlay *et al.*, "TiAl alloys in commercial aircraft engines," *Materials at High Temperatures*, vol. 33, no. 4-5, pp. 549–559, 2016.

[7] R. Gupta, B. Pant, and P. Sinha, "Theory and practice of $\gamma + \alpha_2$ Ti-aluminide: a review," *Transactions of the Indian Institute of Metals*, vol. 67, no. 2, pp. 143–165, 2014.

[8] E. A. Loria, "Gamma titanium aluminides as prospective structural materials," *Intermetallics*, vol. 8, no. 9-11, pp. 1339–1345, 2000.

[9] J. Lapin, "TiAl-based alloys: Present status and future perspectives," in *Conference proceedings METAL*, vol. 19, no. 21.5, 2009, p. 2009.

[10] R. Pflumm, S. Friedle, and M. Schütze, "Oxidation protection of γ-TiAl-based alloys–a review," *Intermetallics*, vol. 56, pp. 1–14, 2015.

[11] X. Wu *et al.*, "Oxidation-induced embrittlement of TiAl alloys," *Intermetallics*, vol. 17, no. 7, pp. 540–552, 2009.

[12] H.-E. Zschau and M. Schütze, *Surface modification by ion implantation to improve the oxidation resistance of materials for high temperature technology.* INTECH Open Access Publisher, 2012.

[13] C. Mogab, A. Adams, and D. L. Flamm, "Plasma etching of Si and SiO_2—the effect of oxygen additions to CF_4 plasmas," *Journal of applied physics*, vol. 49, no. 7, pp. 3796–3803, 1978.

[14] "Superalloys for gas turbine engines-12," in *Introduction to aerospace materials*, 2012, pp. 251–267.

[15] K. Gschneidner Jr *et al.*, "A family of ductile intermetallic compounds," *Nature Materials*, vol. 2, no. 9, p. 587, 2003.

[16] M. Zamanzade, A. Barnoush, and C. Motz, "A review on the properties of iron aluminide intermetallics," *Crystals*, vol. 6, no. 1, p. 10, 2016.

[17] F. Appel, R. Wagner, and V. Kumar, "Intermetallics: Titanium aluminides," in *Reference Module in Materials Science and Materials Engineering*, 2015.

[18] P. J. Masset and M. Schütze, "Thermodynamic assessment of the alloy concentration limits for the halogen effect of TiAl alloys," *Advanced Engineering Materials*, vol. 10, no. 7, pp. 666–674, 2008.

[19] M. Thomas and M.-P. Bacos, "Processing and characterization of TiAl-based alloys: Towards an industrial scale," *AerospaceLab*, vol. 3, pp. p–1, 2011.

[20] P. Bartolotta *et al.*, "The use of cast Ti-48Al-2Cr-2Nb in jet engines," *Jom*, vol. 49, no. 5, pp. 48–50, 1997.

[21] X. Huang *et al.*, "Fatigue crack propagation behavior of Ni-based superalloys after overloading at elevated temperatures," *Progress in Natural Science: Materials International*, vol. 26, no. 2, pp. 197–203, 2016.

[22] A. Materials. (2002) Titanium alloys - physical properties. [Online]. Available: https://www.azom.com/article.aspx?ArticleID=1341

[23] X. Wu, "Review of alloy and process development of TiAl alloys," *Intermetallics*, vol. 14, no. 10-11, pp. 1114–1122, 2006.

[24] S. Kekare and P. Aswath, "Oxidation of TiAl based intermetallics," *Journal of materials science*, vol. 32, no. 9, pp. 2485–2499, 1997.

[25] M. Brady *et al.*, "The role of Cr in promoting protective alumina scale formation by γ-based Ti-Al-Cr alloys — II. oxidation behavior in air," *Acta materialia*, vol. 45, no. 6, pp. 2371–2382, 1997.

[26] S. Taniguchi, T. Shibata, and S. Itoh, "Oxidation behavior of TiAl at high temperatures in purified oxygen," *Materials Transactions, JIM*, vol. 32, no. 2, pp. 151–156, 1991.

[27] V. Chuprina and I. Shalya, "Oxidation of TiAl intermetallic," *Powder Metallurgy and Metal Ceramics*, vol. 46, no. 11-12, pp. 582–588, 2007.

[28] D. Kim1 *et al.*, "Oxidation behaviour of gamma titanium aluminides with or without protective coatings," *International Materials Reviews*, vol. 59, no. 6, pp. 297–325, 2014.

[29] S. Draper and D. Isheim, "Environmental embrittlement of a third generation γ-TiAl alloy," *Intermetallics*, vol. 22, pp. 77–83, 2012.

[30] S. Becker *et al.*, "Mechanism of isothermal oxidation of the intermetallic TiAl and of TiAl alloys," *Oxidation of Metals*, vol. 38, no. 5-6, pp. 425–464, 1992.

[31] S. Qu *et al.*, "Microstructural evolution and high-temperature oxidation mechanisms of a titanium aluminide based alloy," *Acta Materialia*, vol. 148, pp. 300–310, 2018.

[32] I. Plumb and K. Ryan, "A model of the chemical processes occurring in CF_4/O_2 discharges used in plasma etching," *Plasma chemistry and plasma processing*, vol. 6, no. 3, pp. 205–230, 1986.

[33] M. Schütze *et al.*, "The halogen effect in the oxidation of intermetallic titanium aluminides," *Corrosion Science*, vol. 44, no. 2, pp. 303–318, 2002.

[34] A. Donchev *et al.*, "Improvement of the oxidation behaviour of TiAl-alloys by treatment with halogens," *Intermetallics*, vol. 14, no. 10-11, pp. 1168–1174, 2006.

[35] A. Donchev and M. Schütze, "Cyclic oxidation behaviour of halogen implanted Ti-46.5Al-4(Cr, Nb, Ta, B)," in *Materials Science Forum*, vol. 461. Trans Tech Publ, 2004, pp. 447–454.

[36] ——, "Improving the oxidation resistance of γ-titanium aluminides by halogen treatment," *Materials and corrosion*, vol. 59, no. 6, pp. 489–493, 2008.

[37] A. Donchev *et al.*, "Improving the oxidation resistance of TiAl-alloys with fluorine," *Journal of Alloys and Compounds*, vol. 452, no. 1, pp. 7–10, 2008.

[38] ——, "Plasma-immersion-ion-implantation of fluorine to protect TiAl-components against high-temperature oxidation," *Plasma Processes and Polymers*, vol. 6, no. 6-7, pp. 434–439, 2009.

[39] C. Leyens *et al.*, "Recent progress in the coating protection of gamma titanium-aluminides," *Jom*, vol. 58, no. 1, pp. 17–21, 2006.

[40] A. Donchev *et al.*, "The use of fluorine to protect β-solidifying γ-TiAl-based alloys against high-temperature oxidation," *MRS Advances*, vol. 2, no. 25, p. 1361–1367, 2017.

[41] M. Fröhlich, R. Braun, and C. Leyens, "Oxidation resistant coatings in combination with thermal barrier coatings on γ-TiAl alloys for high temperature applications," *Surface and Coatings Technology*, vol. 201, no. 7, pp. 3911–3917, 2006.

[42] C. Wang *et al.*, "Oxidation inhibition of γ-TiAl alloy at 900 °C by inorganic silicate composite coatings," *Corrosion Science*, vol. 76, pp. 284–291, 2013.

[43] M. Ohring, *Materials science of thin films*. Elsevier, 2001.

[44] K. Seshan and D. Schepis, *Handbook of thin film deposition*. William Andrew, 2018.

[45] P. J. Kelly and R. D. Arnell, "Magnetron sputtering: a review of recent developments and applications," *Vacuum*, vol. 56, no. 3, pp. 159–172, 2000.

[46] V. M. Donnelly, "Reactions of fluorine atoms with silicon, revisited, again," *Journal of Vacuum Science & Technology A: Vacuum, Surfaces, and Films*, vol. 35, no. 5, p. 05C202, 2017.

[47] H. F. Winters, J. Coburn, and E. Kay, "Plasma etching a"pseudo-black-box"approach," *Journal of Applied Physics*, vol. 48, no. 12, pp. 4973–4983, 1977.

[48] L. Christophorou, "Electron interactions with CF_4," *J. Phys. Chem. Ref. Data*, vol. 25, p. 1341, 1996.

[49] V. M. Donnelly and A. Kornblit, "Plasma etching: Yesterday, today, and tomorrow," *Journal of Vacuum Science & Technology A: Vacuum, Surfaces, and Films*, vol. 31, no. 5, p. 050825, 2013.

[50] G. F. Bauerfeldt and G. Arbilla, "Kinetic analysis of the chemical processes in the decomposition of gaseous dielectrics by a non-equilibrium plasma-part 1: CF_4 and CF_4/O_2," *Journal of the Brazilian Chemical Society*, vol. 11, no. 2, pp. 121–128, 2000.

[51] I. Chun *et al.*, "A comparative study of $CF_4/O_2/Ar$ and $C_4F_8/O_2/Ar$ plasmas for dry etching applications," *Thin Solid Films*, vol. 579, pp. 136–143, 2015.

[52] Y. Hikosaka, H. Toyoda, and H. Sugai, "Spatial distribution and surface loss of CF_3 and CF_2 radicals in a CF_4 etching plasma," *Japanese journal of applied physics*, vol. 32, no. 3A, p. L353, 1993.

[53] C. Beenakker, J. Van Dommelen, and R. Van De Poll, "Decomposition and product formation in CF_4-O_2 plasma etching silicon in the afterglow," *Journal of Applied Physics*, vol. 52, no. 1, pp. 480–485, 1981.

[54] E. De Hoffmann, "Mass spectrometry," *Kirk-Othmer Encyclopedia of Chemical Technology*, 2000.

[55] J. I. Goldstein *et al.*, *Scanning electron microscopy and X-ray microanalysis*. Springer, 2017.

[56] W.-K. Chu, *Backscattering spectrometry*. Elsevier, 2012.

[57] L.-M. Buchmann *et al.*, "Analysis of a CF_4/O_2 plasma using emission, laser-induced fluorescence, mass, and langmuir spectroscopy," *Journal of Applied Physics*, vol. 67, no. 8, pp. 3635–3640, 1990.

[58] G. Smolinsky and D. Flamm, "The plasma oxidation of CF_4 in a tubular-alumina fast-flow reactor," *Journal of Applied Physics*, vol. 50, no. 7, pp. 4982–4987, 1979.

[59] R. L. Merlino, "Dusty plasmas and applications in space and industry," *Plasma Physics Applied*, vol. 81, pp. 73–110, 2006.

[60] S. Friedle *et al.*, "ToF-SIMS study on the initial stages of the halogen effect in the oxidation of TiAl alloys," *Oxidation of Metals*, vol. 89, no. 1-2, pp. 123–139, 2018.

[61] O. Ostrovskaya *et al.*, "Thermogravimetric investigation on oxidation kinetics of complex Ti-Al alloys," *Intermetallics*, vol. 93, pp. 244–250, 2018.

[62] S. Neve *et al.*, "High temperature oxidation resistance of fluorine-treated TiAl alloys: Chemical vs. ion beam fluorination techniques," *Nuclear Instruments and Methods in Physics Research Section B: Beam Interactions with Materials and Atoms*, vol. 268, no. 21, pp. 3381–3385, 2010.

[63] P. J. Masset and M. Schütze, "Improvement of the oxidation resistance of TiAl alloys using controlled gaseous fluorination," *ECS Transactions*, vol. 11, no. 15, pp. 37–48, 2008.

[64] X. Gong *et al.*, "Effect of Mo on microstructure and oxidation of NiCoCrAlY coatings on high Nb-containing TiAl alloys," *Applied Surface Science*, vol. 431, pp. 81 – 92, 2018, 5th Asian Conference on Heat Treatment and Surface Engineering. [Online]. Available: http://www.sciencedirect.com/science/article/pii/S0169433217320160

[65] K. Zhang, T. Zhang, and L. Song, "Oxidation behavior of a high-Nb-containing TiAl alloy with multilayered thermal barrier coatings," *Journal of Thermal Spray Technology*, vol. 27, no. 6, pp. 999–1010, Aug 2018. [Online]. Available: https://doi.org/10.1007/s11666-018-0736-9

[66] D. Y. Seo, T. D. Nguyen, and D. B. Lee, "Oxidation of powder metallurgy (PM) Ti-48%Al-2%Cr-2%Nb-(0-1%)W alloys between 800 and 1000 °C in air," *Oxidation of Metals*, vol. 74, no. 3, pp. 145–156, Oct 2010. [Online]. Available: https://doi.org/10.1007/s11085-010-9203-9

[67] A. Donchev *et al.*, "Optimization of the fluorine effect for improving the oxidation resistance of TiAl-alloys," in *Materials Science Forum*, vol. 706. Trans Tech Publ, 2012, pp. 1061–1065.

[68] R. A. Yankov *et al.*, "Microstructural studies of fluorine-implanted titanium aluminides for enhanced environmental durability," *Advanced Engineering Materials*, vol. 16, no. 1, pp. 52–59, 2014.

[69] H.-E. Zschau *et al.*, "Investigation of the fluorine microalloying effect in the oxidation of TiAl at 900°C in air," *Oxidation of Metals*, vol. 59, no. 1-2, pp. 183–200, 2003.

[70] G. Schumacher *et al.*, "Improvement of the oxidation resistance of gamma titanium aluminides by microalloying with chlorine using ion implantation," *Materials and Corrosion*, vol. 50, no. 3, pp. 162–165, 1999.

[71] ——, "Microalloying effects in the oxidation of TiAl materials," *Intermetallics*, vol. 7, no. 10, pp. 1113–1120, 1999.